Angewandte Chemie
Eine Zeitschrift der Gesellschaft Deutscher Chemiker

Supporting Information

Building up Strain in One Step: Synthesis of an Edge-Fused Double Silacyclobutene from an Extensively Trichlorosilylated Butadiene Dianion

*Isabelle Georg, Markus Bursch, Julius B. Stückrath, Edith Alig, Michael Bolte, Hans-Wolfram Lerner, Stefan Grimme, and Matthias Wagner**

anie_202006463_sm_miscellaneous_information.pdf

Table of contents:

1. Experimental details and characterization data

General considerations. All reactions were carried out under an inert-gas atmosphere (dry argon or nitrogen) using standard Schlenk or glove box techniques. Commercially available substances were used as received. Reaction solvents were dried over sodium (*n*-hexane, *n*-pentane, Et_2O) or CaH_2 (CH_2Cl_2) and freshly distilled prior to use. CD_2Cl_2 and [D_8]THF were stored over molecular sieves (4 Å). NMR spectra were recorded on a Bruker Avance III HD 500 spectrometer (equipped with a Prodigy BBO 500 S1 probe). $^{1}H/^{13}C\{^{1}H\}$ NMR spectra were referenced against (residual) solvent signals (CD_2Cl_2: 5.32 ppm/53.84 ppm, [D_8]THF: 3.58 ppm/67.21 ppm;[S1] s = singlet, d = doublet, t = triplet, m = multiplet, br = broad). ^{29}Si NMR spectra were calibrated against external $Si(CH_3)_4$ ($\delta(^{29}Si)$ = 0); whenever present, $SiCl_4$ ($\delta(^{29}Si)$= −18.9)[S2] was used as internal standard. ^{29}Si NMR spectra were acquired by using the pulse sequence zg with a pulse length of 13.0 µs and a relaxation delay of 2.0 s. UV/vis absorption spectra were recorded at room temperature using a Varian Cary 50 Scan UV/vis spectrophotometer. The cyclic voltammogram was recorded at room temperature in a one-chamber, three electrode cell using an EG&G Princeton Applied Research 263A potentiostat with a platinum disk working electrode (diameter 2.00 mm). The reference electrode was a silver wire on which AgCl had been deposited by immersing the wire into HCl/HNO_3 (3:1). [nBu$_4$N][B(C_6F_5)$_4$] was employed as the supporting electrolyte. All potential values are referenced against the FcH/FcH^+ redox couple (FcH = ferrocene; $E_{1/2}$ = 0 V). GC-MS (gas chromatography – mass spectrometry) data were recorded using a Shimadzu GCMS-QP 2010SE. The stationary phase (Restek) had a length of 60 m with an inner diameter of 0.32 mm. The analyte was diluted with CH_2Cl_2 prior to the measurement. To avoid overloading the MS, a solvent cut was used. Samples were injected at 200 °C and 1/10 thereof was transferred onto column with a flow rate of 1.86 mL/min, carried by helium gas. The oven was heated from 50 °C for 1 min, the temperature was subsequently elevated at a rate of 20 °C/min up to 220 °C and held for 40 min, then elevated again at a rate of 30 °C/min up to 270 °C and held for 5 min. After exiting the column, substances were ionized with 70 eV and cationic fragments were measured within a range of m/z = 30-900 (mass per charges). The melting point was determined using an OptiMelt MPA 100 apparatus.

Note: **In the reaction protocols compiled below, the reaction equations show the theoretically required stoichiometries of the individual reactants, which can slightly deviate from the stoichiometries used in practice, mainly for reasons of convenience.**

Synthesis of [*n*Bu$_4$N]$_2$[1].

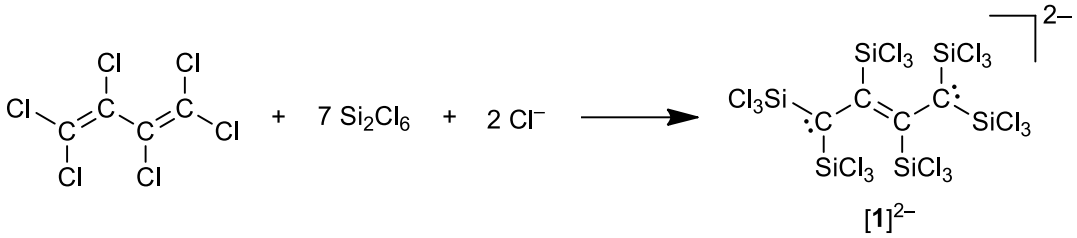

In the glove box, neat Si_2Cl_6 (4.62 mL, 7.22 g, 26.9 mmol) was added dropwise with stirring at room temperature to a glass vessel, charged with a solution of [*n*Bu$_4$N]Cl (2.13 g, 7.66 mmol) and C_4Cl_6 (0.997 g, 3.82 mmol) in CH_2Cl_2 (18 mL). After stirring for 12 h at room temperature, [*n*Bu$_4$N]$_2$[**1**] precipitated as a bright yellow solid. The product was isolated by filtration and washed with an Et_2O-CH_2Cl_2 mixture (4:1, 10 × 1 mL). Yellow crystals of [*n*Bu$_4$N]$_2$[**1**] suitable for X-ray analysis were obtained through recrystallization from warm CH_2Cl_2. Yield (crystals): 1.83 g (1.37 mmol, 36%).

^{1}H NMR (500.2 MHz, [D$_8$]THF, 298 K): δ = 3.34 (m, 16H; C*H*$_2$N), 1.72 (m, 16H; C*H*$_2$CH$_2$N), 1.44 (m, 16H; CH$_3$C*H*$_2$), 1.02 ppm (t, $^3J_{HH}$ = 7.4 Hz, 24H; C*H*$_3$).

^{13}C{^{1}H} NMR (125.8 MHz, [D$_8$]THF, 298 K): δ = 159.7 (*C*=), 59.2 (*C*H$_2$N), 50.2 (*C*(SiCl$_3$)$_2$), 24.6 (*C*H$_2$CH$_2$N), 20.4 (CH$_3$*C*H$_2$), 13.9 ppm (*C*H$_3$).

^{29}Si NMR (99.4 MHz, [D$_8$]THF, 298 K): δ = –13.1 ((Cl$_3$*Si*)$_2$C–), –15.8 ppm (Cl$_3$*Si*C=).

Synthesis of 2.

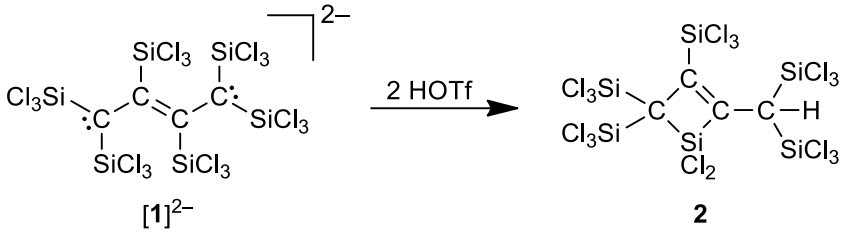

$[\mathbf{1}]^{2-}$ **2**

In the glove box, neat HO_3SCF_3 (HOTf; 0.180 g, 1.20 mmol) was added dropwise with stirring at room temperature to a small glass vessel, charged with a yellow suspension of $[n\mathrm{Bu_4N}]_2[\mathbf{1}]$ (0.655 g, 0.489 mmol) in *n*-hexane (6 mL). The reaction mixture was stirred for 15 min at room temperature, after which time the yellow color had vanished and a small amount of grey insoluble material stuck to the glass wall. The liquid phase was transferred to a Schlenk flask via syringe and the sticky residue extracted with *n*-hexane (4 × 1 mL). The combined *n*-hexane solutions were evaporated under reduced pressure to furnish a colorless solid; colorless single crystals of **2** suitable for X-ray analysis were obtained through slow evaporation of an *n*-pentane solution. Yield (crystals): 0.368 g (0.449 mmol, 92%).

^{1}H NMR (500.2 MHz, CD_2Cl_2, 298 K): δ = 4.00 ppm (s, $^2J_{HSi}$ = 13.4 Hz, $^3J_{HSi}$ = 21.1 Hz, $^4J_{HSi}$ = 7.8 Hz, 1H; $(Cl_3Si)_2C\mathit{H}$).

^{13}C{^{1}H} NMR (125.8 MHz, CD_2Cl_2, 298 K): δ = 163.8 (*C*=C)*, 155.3 (*C*=C)*, 55.0 ($(Cl_3Si)_2\mathit{C}$–$SiCl_2$), 42.5 ppm ($(Cl_3Si)_2\mathit{C}H$). *) Both resonances gave cross peaks of comparable intensity in the ^{13}C HMBC experiment; an unambiguous assignment of the two olefinic C atoms was therefore not possible.

^{29}Si NMR (99.4 MHz, CD_2Cl_2, 298 K): δ = –0.7 ($(Cl_3\mathit{Si})_2C$), –2.0 (d, $^2J_{SiH}$ = 13.4 Hz; $(Cl_3\mathit{Si})_2CH$), –10.6 (d, $^3J_{SiH}$ = 21.1 Hz; $\mathit{Si}Cl_2$), –14.5 ppm ($Cl_3\mathit{Si}$–C=).

Justification for the assignment of the ^{29}Si resonances: The signals at –0.7 and –2.0 ppm possess larger integral values than the other two resonances and their chemical shifts are closer to those of the Cl_3Si groups in $(Cl_3Si)_2HC$–$CH(SiCl_3)_2$ (H_2**B**; δ = 3.0/4.1 ppm).[S3] The two lower-field signals can thus be assigned to the $(Cl_3\mathit{Si})_2C$ and $(Cl_3\mathit{Si})_2CH$ fragments. The signal at –2.0 ppm shows fully resolved J_{SiH} coupling and is likely associated with the $(Cl_3\mathit{Si})_2CH$ group, because $^2J_{SiH}$ coupling constants should be larger than $^5J_{SiH}$ coupling constants. The assignment of the remaining two resonances is somewhat speculative and essentially based on the assumption that $^3J_{SiH} > {}^4J_{SiH}$.

Reaction of 2 with [*n*Bu$_4$N]Cl.

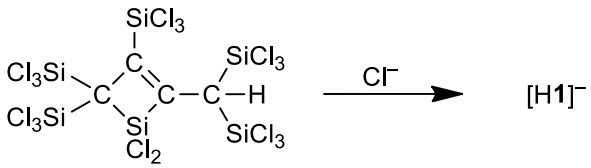

2

In the glove box, an NMR tube was charged with neat [*n*Bu$_4$N]Cl (0.011 g, 0.040 mmol) and a solution of **2** (0.032 g, 0.039 mmol) in CD_2Cl_2 (0.5 mL). The tube was flame-sealed under vacuum. The ^{1}H, ^{13}C{^{1}H}, and ^{29}Si NMR spectra of the yellow solution revealed a complete conversion to one single product, *i.e.*, the monoprotonated species [H**1**]$^-$. The same signal set is reproducibly observed (together with the resonances of **2**) when [**1**]$^{2-}$ is treated with less than 2 equiv of HOTf.

^{1}H NMR (500.2 MHz, CD_2Cl_2, 298 K): δ = 3.16 ppm (s, $^2J_{HSi}$ = 11.3 Hz, $^4J_{HSi}$ = 5.8 Hz, 1H; $(Cl_3Si)_2CH$), 3.12 (m, 8H; CH_2N), 1.62 (m, 8H; CH_2CH_2N), 1.44 (m, 8H; CH_3CH_2), 1.03 ppm (t, $^3J_{HH}$ = 7.4 Hz, 12H; CH_3).

^{13}C{^{1}H} NMR (125.8 MHz, CD_2Cl_2, 298 K): δ = 176.4 (*C*=C)*, 114.1 (*C*=C)*, 70.1 ($(Cl_3Si)_2C$–$SiCl_3$–), 59.5(CH_2N), 43.3 ($(Cl_3Si)_2CH$), 24.3 (CH_2CH_2N), 20.1 (CH_3CH_2), 13.8 ppm (CH_3). *) Both resonances gave cross peaks of comparable intensity in the ^{13}C HMBC experiment; an unambiguous assignment of the two olefinic C atoms was therefore not possible.

^{29}Si NMR (99.4 MHz, CD_2Cl_2, 298 K): δ = 4.9 (d, J_{SiH} = 5.8 Hz), –17.3, –18.7 ppm (br/d, J_{SiH} = 11.3 Hz).

Comments regarding the NMR data: The signal at –18.7 ppm possesses the largest integral value and shows well-resolved J_{SiH} coupling (11.3 Hz). The signal collapses to a singlet in the ^{29}Si{^{1}H} NMR spectrum. Under these measurement conditions a second resonance in the immediate vicinity is resolved, which explains the large overall integral value mentioned above. Of the two remaining resonances, only the one at 4.9 ppm possesses a clear-cut doublet multiplicity (J_{SiH} = 5.8 Hz). We also note that two pairs of ^{29}Si satellites are visible in the ^{1}H NMR spectrum of [H**1**]$^-$: the one corresponding to J_{SiH} = 11.3 Hz is approximately double as high as the one corresponding to J_{SiH} = 5.8 Hz, which further indicates that the latter coupling originates from one rather than two magnetically equivalent $SiCl_3$ groups. The fact, that the protonated C atom possesses a chemical shift value of δ(^{13}C) = 43.3 ppm was confirmed by means of a HSQC experiment.

Structure proposals for [H1]$^-$: Figure S1a shows three conceivable isomers of [H**1**]$^-$, the terminally protonated [H**1**]^-_t, the internally protonated [H**1**]^-_i, and the cyclic adduct [H**1**]^-_c. Quantum-chemical calculations on these three anions (without their accompanying non-coordinating [*n*Bu$_4$N]$^+$ cations) were performed at the PBE0-D4+COSMO-RS(CH_2Cl_2)/def2-QZVPPD//PBE0-D4(COSMO(CH_2Cl_2))/def2-TZVPD level of theory. Compared to the internally protonated isomer

$[H\mathbf{1}]^-_i$ as the reference (ΔG = 0 kcal·mol^{-1}), $[H\mathbf{1}]^-_t$ and $[H\mathbf{1}]^-_c$ are thermodynamically favored by –29.7 kcal·mol^{-1} and –32.4 kcal·mol^{-1}, respectively. This likely excludes $[H\mathbf{1}]^-_i$ as the species present in CH_2Cl_2 solution. The resonance with the most negative chemical shift value that we are observing for $[H\mathbf{1}]^-$ appears at $\delta(^{29}Si)$ = –19 ppm. Given that only a significantly more negative chemical shift would be indicative for pentacoordinate Si atoms, the open-chain isomer $[H\mathbf{1}]^-_t$ currently remains as the most reasonable structural proposal (cf. Ref[S4]: "Generally higher coordination numbers result in an upfield move of the silicon chemical shift."; quantum-chemical calculations on $[H\mathbf{1}]^-_c$ at the SO-ZORA-PBE0(COSMO(CH_2Cl_2))/ZORA/QZ4P//PBE0-D4(COSMO(CH_2Cl_2))/def2-TZVPD level of theory predict a chemical shift value of –107.7 ppm for the endocyclic Si atom). Indeed, as shown in Figures S1b and S38, we can assign all observed NMR signals to $[H\mathbf{1}]^-_t$ in a way that their chemical shift values fit reasonably well to those of the available model systems and the calculated data. However, the following inconsistencies persist: (i) If the resonance at 4.9 ppm really corresponded to two $SiCl_3$ groups, one would expect a higher signal intensity; (ii) a value of 5.8 Hz is rather small for a $^2J_{SiH}$ coupling constant; (iii) the intensity of the doublet currently assigned to a single $SiCl_3$ group is unusually large.

(a)

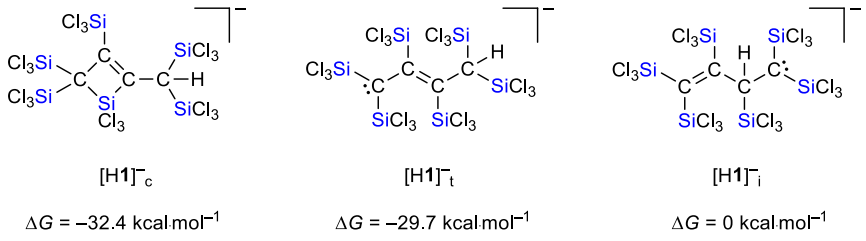

(b)

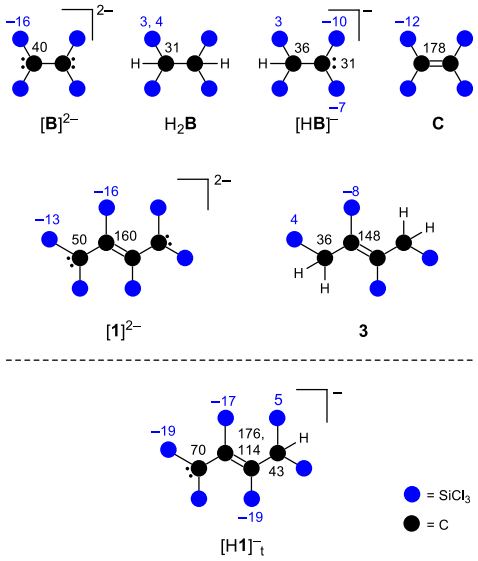

Figure S1: (a) Three possible isomers of $[H\mathbf{1}]^-$: the cyclic adduct $[H\mathbf{1}]^-_c$, the terminally protonated $[H\mathbf{1}]^-_t$, and the internally protonated $[H\mathbf{1}]^-_i$, with their Gibbs free energies relative to $[H\mathbf{1}]^-_i$ at the PBE0-D4+COSMO-RS(CH_2Cl_2)/def2-QZVPPD//PBE0-D4(COSMO(CH_2Cl_2))/def2-TZVPD level of theory. (b) Tentative assignments of the NMR resonances observed for $[H\mathbf{1}]^-$ to the terminally protonated open-chain isomer $[H\mathbf{1}]^-_t$.

Synthesis of 3.

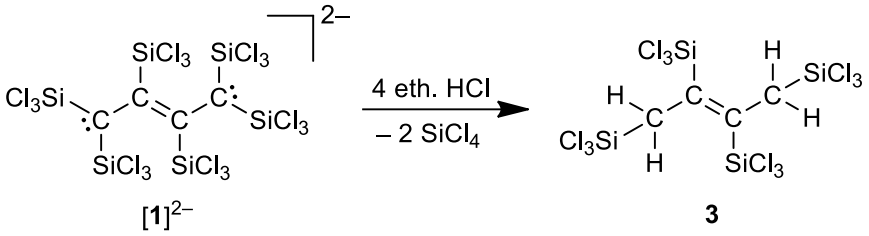

$[\mathbf{1}]^{2-}$ **3**

A solution of HCl in Et_2O (2 M, 2.1 mL, 4.2 mmol) was added with stirring at room temperature to a Schlenk flask containing a yellow suspension of $[n\mathrm{Bu_4N}]_2[\mathbf{1}]$ (1.00 g, 0.746 mmol) in CH_2Cl_2 (10 mL). After stirring at room temperature for 18 h, a pale-yellow solution had formed. All volatiles were removed under reduced pressure (the presence of $SiCl_4$ in the condensate was confirmed by ^{29}Si NMR spectroscopy). The pale-yellow, oily residue was extracted with *n*-hexane (1 × 10 mL, 12 × 3 mL), and the combined extracts were evaporated under reduced pressure to furnish the crude product. The crude product was dissolved in *n*-pentane (1 mL) and the volume of the solution reduced by slow evaporation under ambient pressure. A colorless solid and a yellow supernatant formed, which was removed via syringe. The solid residue was washed with a few drops of *n*-pentane and dried under vacuum to obtain **3** as a colorless solid. Yield: 0.193 g (0.327 mmol, 44%). Single crystals of **3** suitable for X-ray analysis were grown through slow evaporation of a solution in *n*-pentane.

^{1}H NMR (500.2 MHz, CD_2Cl_2, 298 K): δ = 3.49 ppm (s, $^2J_{HSi} \approx {}^3J_{HSi} \approx$ 13 Hz, 4H; CH_2).

^{13}C{^{1}H} NMR (125.8 MHz, CD_2Cl_2, 298 K): δ = 147.8 (C=), 36.4 ppm (CH_2).

^{29}Si NMR (99.4 MHz, CD_2Cl_2, 298 K): δ = 4.1 (t, $^2J_{SiH}$ = 13.0 Hz; Cl_3SiCH_2), –7.8 ppm (t, $^3J_{SiH}$ = 12.5 Hz; Cl_3SiC=).

GC-MS (EI): rt = 32.48 min, *m*/*z* = 590 ($[M]^+$).

Synthesis of 4.

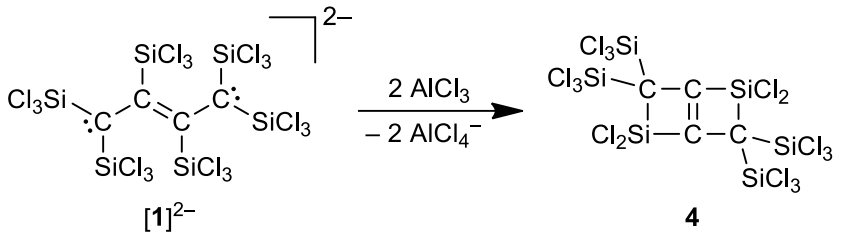

$[\mathbf{1}]^{2-}$ **4**

In a glove box, neat $AlCl_3$ (0.125 mg, 0.937 mmol) was added with stirring at room temperature to a Schlenk flask containing a yellow suspension of [*n*Bu_4N]$_2$[**1**] (0.500 g, 0.373 mmol) in CH_2Cl_2 (5 mL). The reaction mixture was stirred for 2.5 h, whereupon the yellow color vanished, and the amount of insoluble material decreased. The solvent was evaporated under reduced pressure and the solid residue extracted with *n*-hexane (11 × 1 mL). The combined extracts were evaporated under reduced pressure to obtain **4** as a colorless solid. Yield: 0.245 g (0.313 mmol, 84%). Single crystals of **4** suitable for X-ray analysis were grown from a solution in CH_2Cl_2.

^{13}C{^{1}H} NMR (125.8 MHz, CD_2Cl_2, 298 K): δ = 175.6 ppm (*C*=); n.o. ($Cl_3Si)_2$*C*–C= (despite extended relaxation times). *Note:* The chemical shift value of the missing ^{13}C NMR signal was computed at the SO-ZORA-PBE0(COSMO(CH_2Cl_2))/ZORA/QZ4P//PBE0-D4(COSMO(CH_2Cl_2))/def2-TZVP level of theory (59.7 ppm). See the Computational details section for more details.

^{29}Si NMR (99.4 MHz, CD_2Cl_2, 298 K): δ = –2.3 (*Si*Cl_3), –11.9 ppm (*Si*Cl_2).

Reaction of 4 with [*n*Bu$_4$N]Cl.

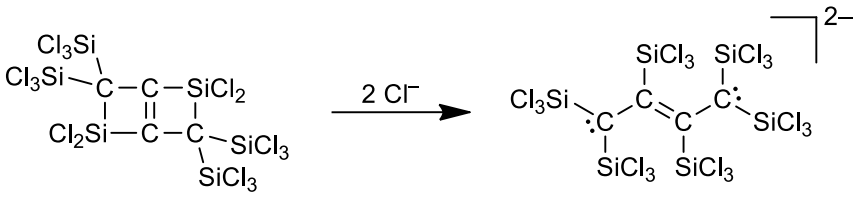

4 [**1**]$^{2-}$

In the glove box, an NMR tube was charged with **4** (0.030 g, 0.038 mmol) and [*n*Bu$_4$N]Cl (0.021 g, 0.076 mmol). Upon addition of CD_2Cl_2 (0.5 mL), an orange solution formed and after a few minutes, a yellow solid precipitated. The tube was flame-sealed under vacuum. An NMR spectroscopic investigation showed the complete disappearance of the resonances of **4**. After the measurement, the NMR tube was heated to 50 °C until the solid had completely dissolved and then slowly cooled to room temperature again, whereupon yellow single crystals grew. The NMR tube was opened inside the glove box, the crystals were isolated by filtration, dried, and identified as [*n*Bu$_4$N]$_2$[**1**] by single crystal X-ray analysis and powder X-ray diffraction. Yield (crystals): 0.044 g (0.033 mmol, 87%).

See above for characterization details of [*n*Bu$_4$N]$_2$[**1**].

Reaction of 4 with eth. HCl.

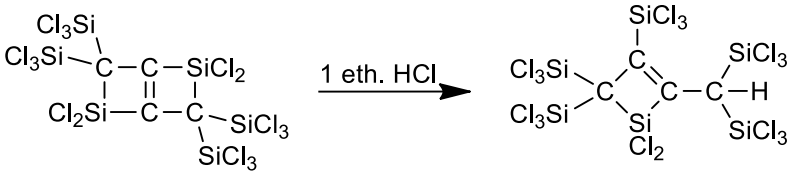

4 **2**

A solution of HCl in Et_2O (2 M, 0.05 mL, 0.10 mmol) was added to an NMR tube charged with a solution of **4** (0.031 g, 0.040 mmol) in CD_2Cl_2 (0.5 mL). The tube was flame-sealed under vacuum. The ^{1}H, $^{13}C\{^{1}H\}$, and ^{29}Si NMR spectra of the colorless solution revealed a clean conversion to **2** as the exclusive product.

See above for characterization details of **2**.

Reaction of 2 with Cl^- and eth. HCl.

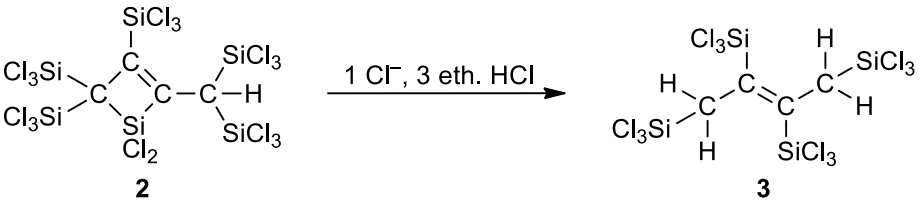

2 **3**

A solution of HCl in Et_2O (2 M, 0.05 mL, 0.10 mmol) was added to an NMR tube charged with a solution of **2** (0.026 g, 0.032 mmol) and $[Ph_4P]Cl$ (0,012 g, 0,032 mmol) in CD_2Cl_2 (0.5 mL). The tube was flame-sealed under vacuum. The ^{1}H, $^{13}C\{^{1}H\}$, and ^{29}Si NMR spectra of the colorless solution revealed a clean conversion to **3** as the exclusive product.

See above for characterization details of **3**.

Note: $[Ph_4P]Cl$ can used similar to $[nBu_4N]Cl$ as soluble Cl^- ion source.

Reaction of [*n*Bu$_4$N]$_2$[1] with 1 equiv AlCl$_3$ and subsequent reaction with HOTf.

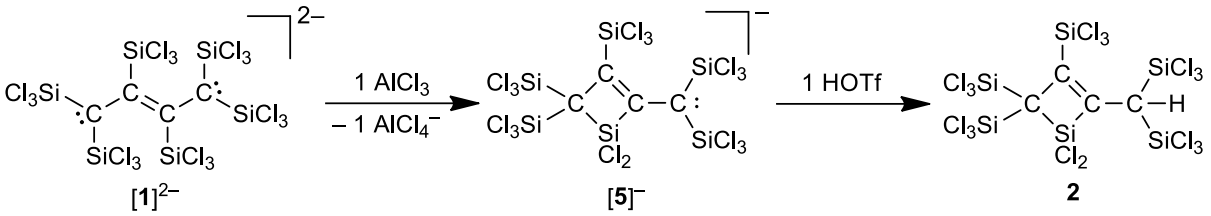

[**1**]$^{2-}$ [**5**]$^{-}$ **2**

In the glove box, an NMR tube was charged with [*n*Bu$_4$N]$_2$[**1**] (0.080 g, 0.060 mmol), AlCl$_3$ (0.008 g, 0.060 mmol), and CD$_2$Cl$_2$ (0.5 mL). The tube was flame-sealed under vacuum. The ^{1}H, ^{13}C{^{1}H}, and ^{29}Si NMR spectra of the orange reaction mixture showed only one set of signals which can be assigned to compound [**5**]$^{-}$. The NMR tube was opened inside the glove box, transferred into a new NMR tube, and the reaction mixture was treated with HOTf (0.012 g, 0.080 mmol). The tube was flame-sealed under vacuum. The ^{1}H, ^{13}C{^{1}H}, and ^{29}Si NMR spectra of the pale-yellow reaction solution revealed a clean conversion to **2** as the exclusive product.

Compound [**5**]$^{-}$:

^{1}H NMR (500.2 MHz, CD$_2$Cl$_2$, 298 K): δ = 3.10 (m, 8H; C*H*$_2$N), 1.62 (m, 8H; C*H*$_2$CH$_2$N), 1.44 (m, 8H; CH$_3$C*H*$_2$), 1.02 ppm (t, $^{3}J_{HH}$ = 7.4 Hz, 12H; C*H*$_3$).

^{13}C{^{1}H} NMR (125.8 MHz, CD$_2$Cl$_2$, 298 K): δ = 181.9 (*C*=C), 134.0(*C*=C), 62.8 ((Cl$_3$Si)$_2$*C*–SiCl$_3$–), 59.4 (*C*H$_2$N), 51.7 ((Cl$_3$Si)$_2$*C*$^{-}$), 24.2 (*C*H$_2$CH$_2$N), 20.0 (CH$_3$*C*H$_2$), 13.7 ppm (*C*H$_3$).

^{29}Si NMR (99.4 MHz, CD$_2$Cl$_2$, 298 K): δ = –0.1 ((Cl$_3$*Si*)$_2$C), –12.5 (*Si*Cl$_2$), –15.6 ((Cl$_3$*Si*)$_2$C^{-}), –16.1 ppm (Cl$_3$*Si*–C=).

See above for characterization details of **2**.

Reaction of [*n*Bu$_4$N]$_2$[1] with 1 equiv AlCl$_3$ and subsequent reaction with 1 equiv [Ph$_4$P]Cl.

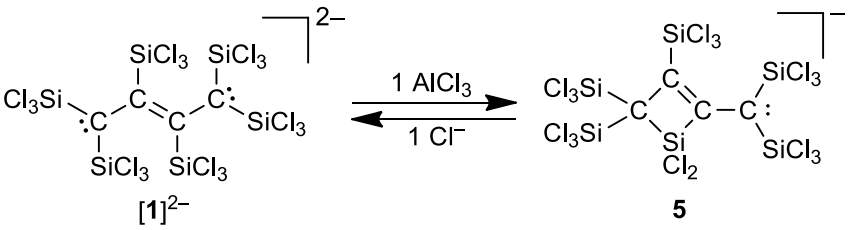

[**1**]$^{2–}$ **5**

In the glove box, an NMR tube was charged with [*n*Bu$_4$N]$_2$[**1**] (0.050 g, 0.037 mmol), AlCl$_3$ (0.005 g, 0.038 mmol), and CD$_2$Cl$_2$ (0.5 mL). The tube was flame-sealed under vacuum. The ^{1}H, ^{13}C{^{1}H}, and ^{29}Si NMR spectra of the orange reaction mixture showed only one set of signals which can be assigned to compound [**5**]$^–$. The NMR tube was opened inside the glove box, transferred into a new NMR tube which was charged with [Ph$_4$P]Cl (0.014 g, 0.037 mmol). The tube was flame-sealed under vacuum. An NMR spectroscopic investigation showed the disappearance of the resonances of [**5**]$^–$. The NMR tube was opened inside the glove box, and upon slow evaporation of the solvent yellow single crystals of [Ph$_4$P]$_2$[**1**] suitable for X-ray analysis were obtained.

2. Plots of ^{1}H, $^{13}C\{^{1}H\}$, and ^{29}Si NMR spectra

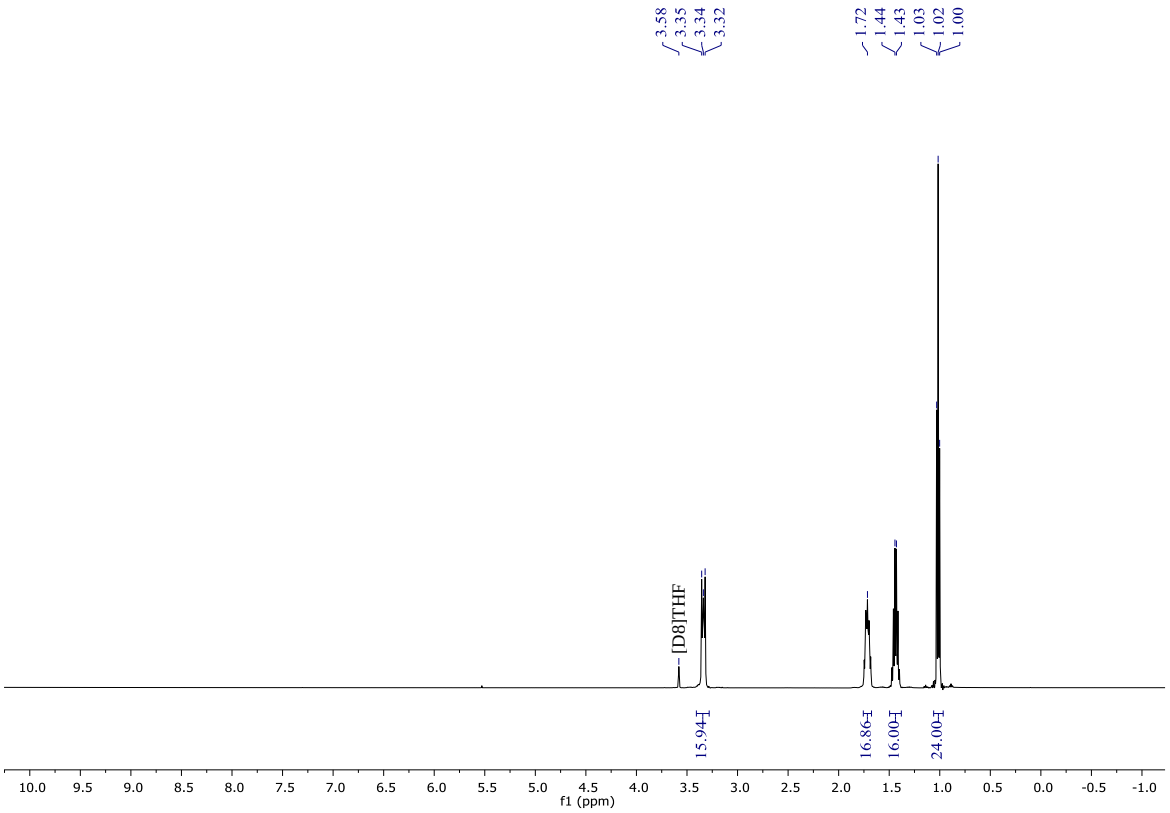

Figure S2: ^{1}H NMR spectrum of [nBu$_4$N]$_2$[**1**] ([D$_8$]THF, 500.2 MHz).

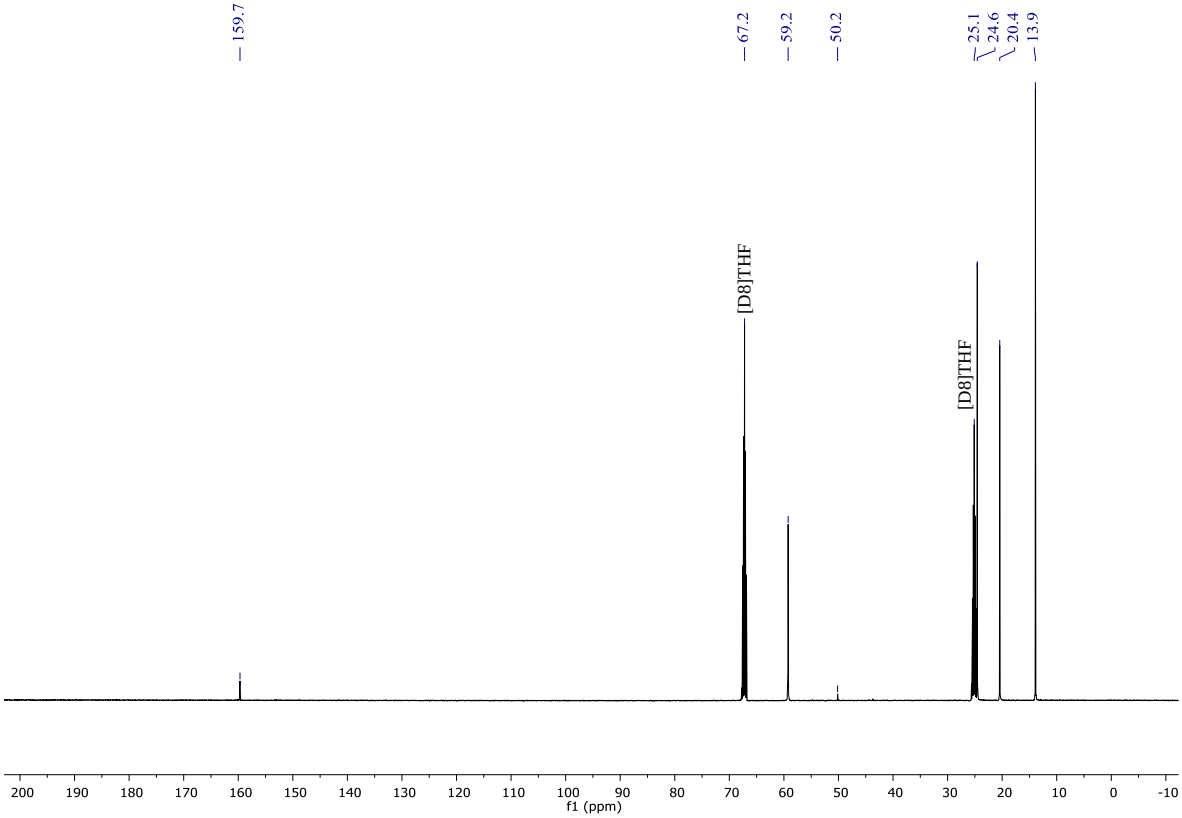

Figure S3: $^{13}C\{^{1}H\}$ NMR spectrum of [nBu$_4$N]$_2$[**1**] ([D$_8$]THF, 125.8 MHz).

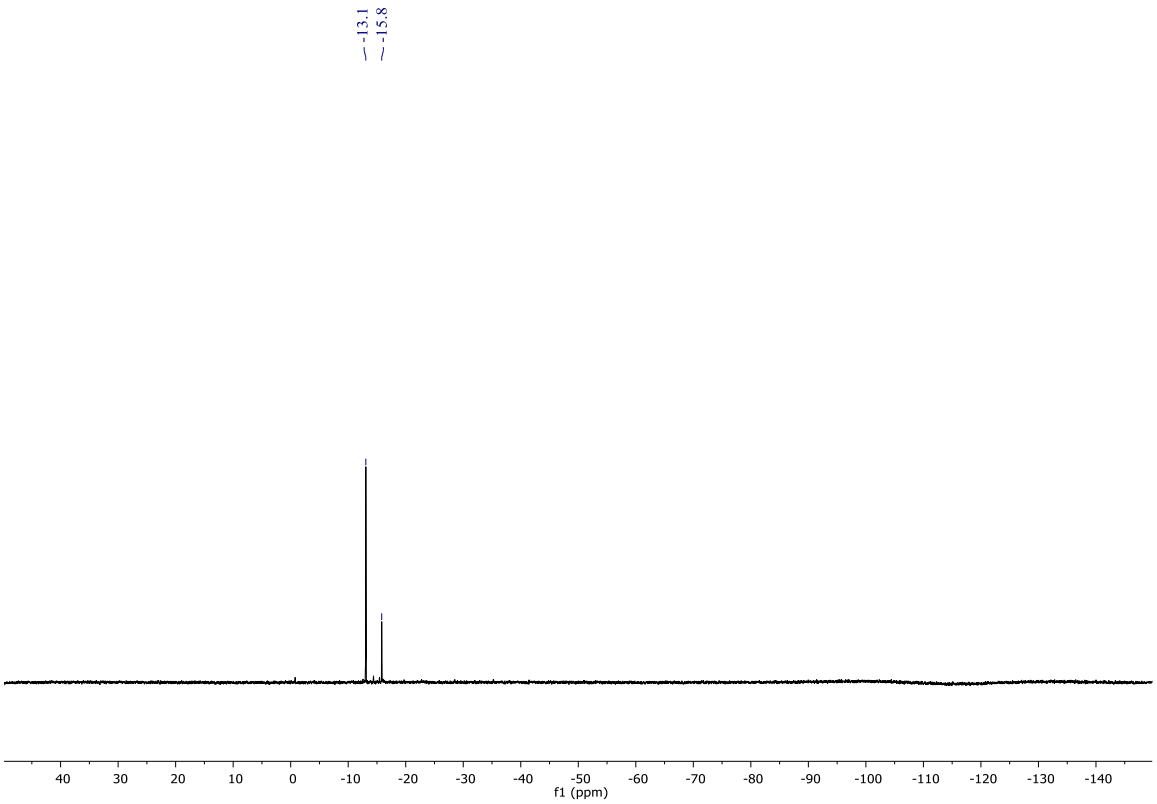

Figure S4: ^{29}Si NMR spectrum of [*n*Bu$_4$N]$_2$[**1**] ([D$_8$]THF, 99.4 MHz).

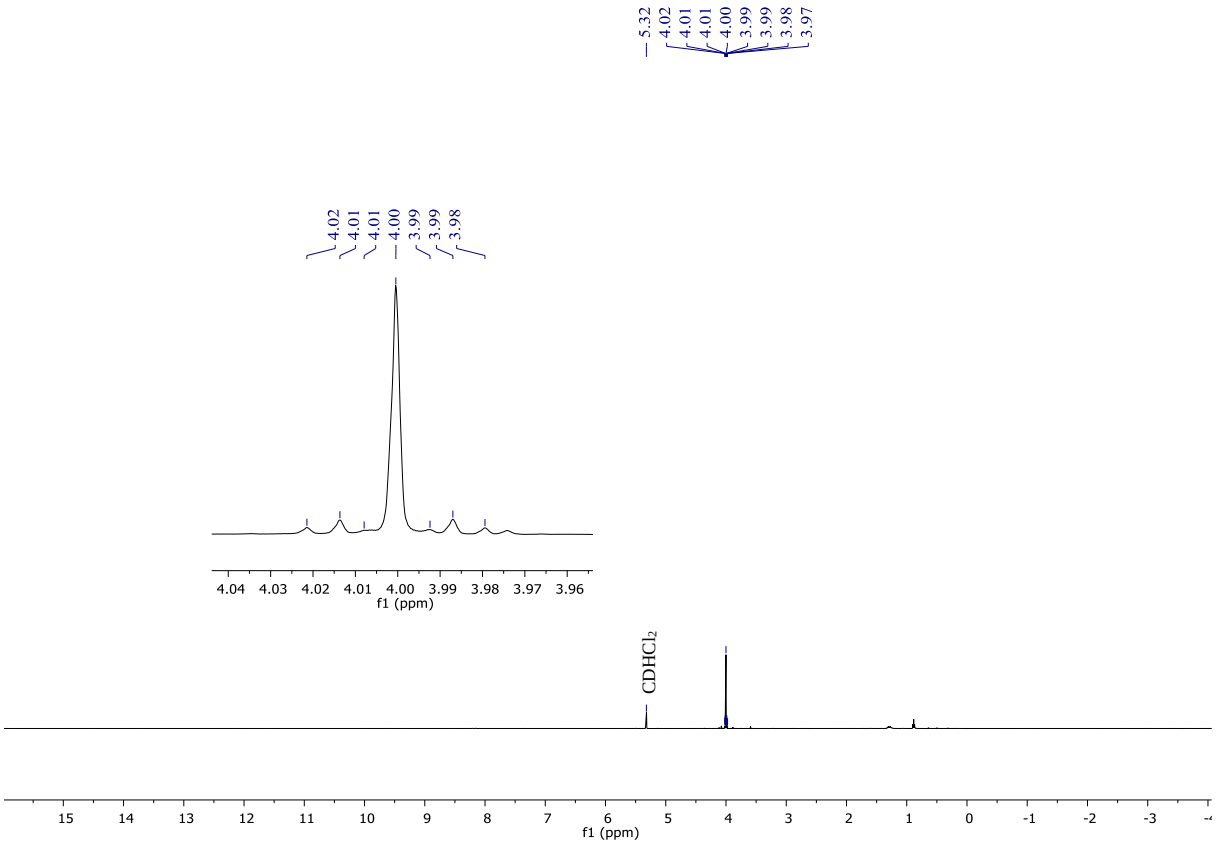

Figure S5: ^{1}H NMR spectrum of **2** (CD_2Cl_2, 500.2 MHz).

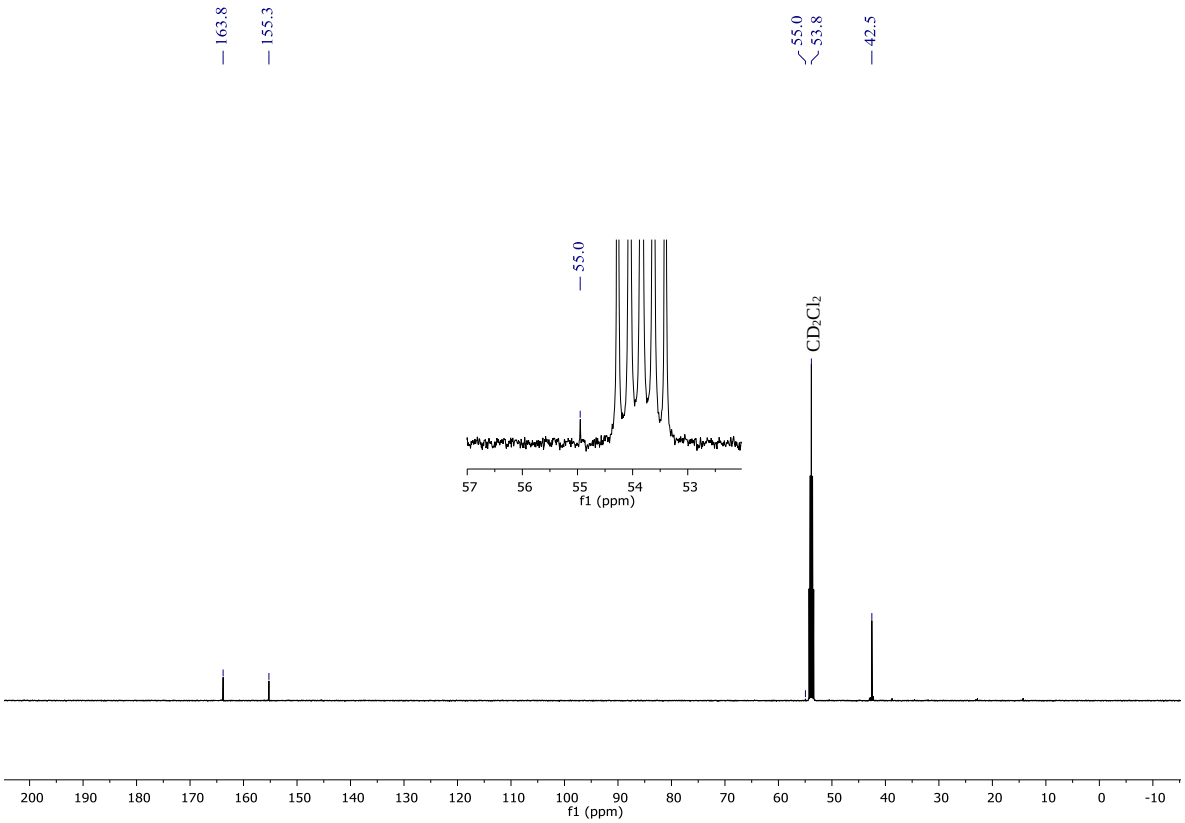

Figure S6: $^{13}C\{^{1}H\}$ NMR spectrum of **2** (CD_2Cl_2, 125.8 MHz).

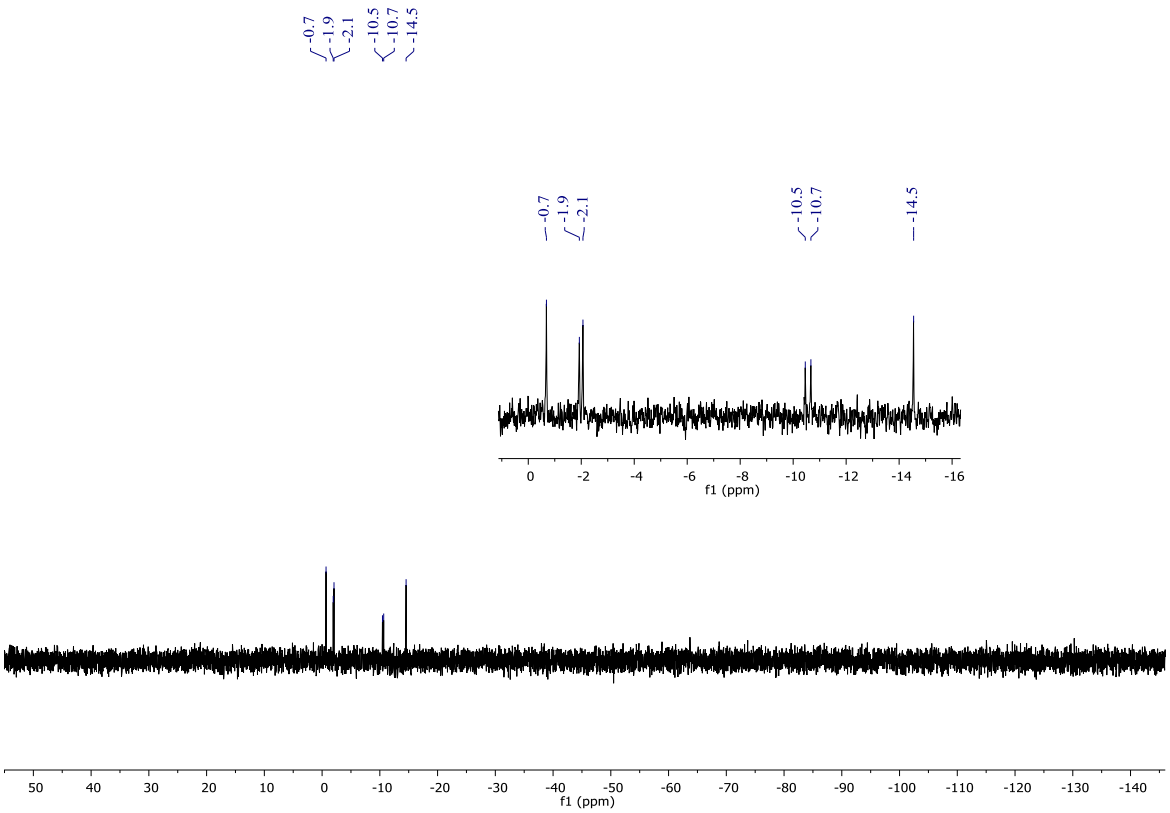

Figure S7: ^{29}Si NMR spectrum of **2** (CD_2Cl_2, 99.4 MHz).

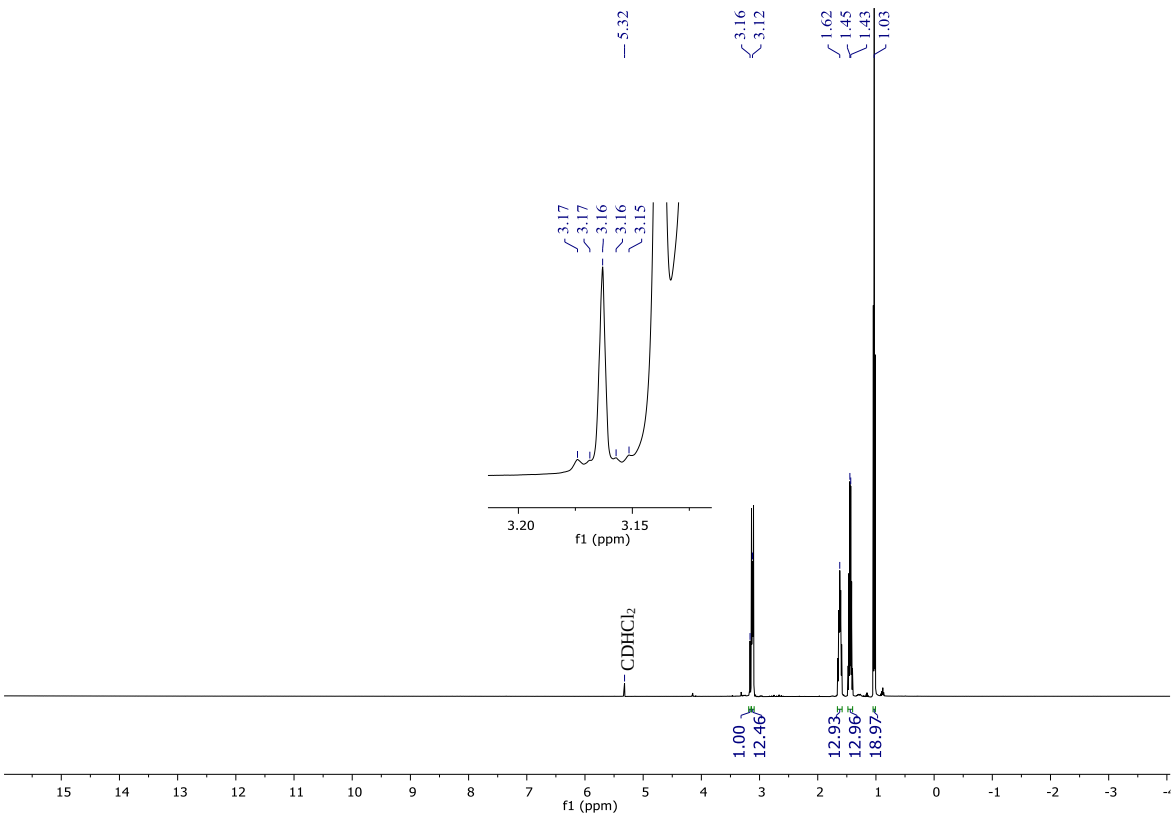

Figure S8: ^{1}H NMR spectrum of the reaction mixture of **2** with [*n*Bu$_4$N]Cl, which furnishes the monoprotonated species [H**1**]$^-$ (CD_2Cl_2, 500.2 MHz).

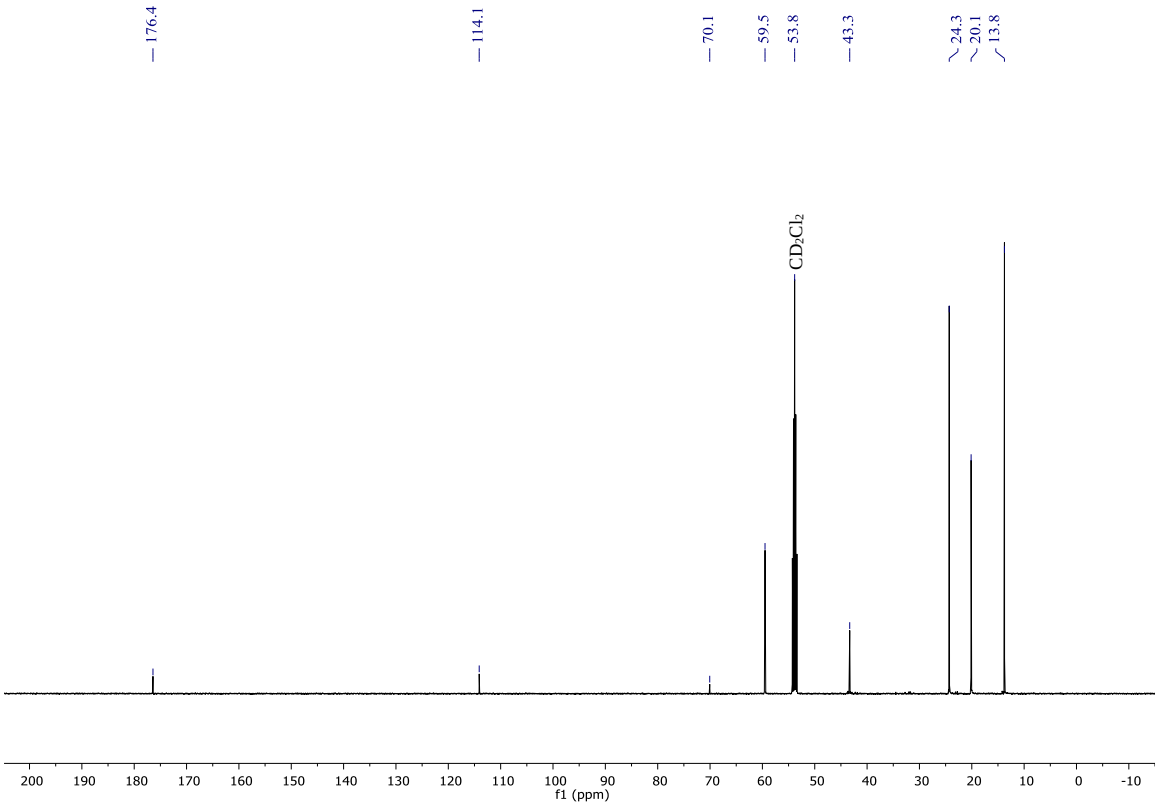

Figure S9: $^{13}C\{^{1}H\}$ NMR spectrum of the reaction mixture of **2** with [*n*Bu$_4$N]Cl, which furnishes the monoprotonated species [H**1**]$^-$ (CD_2Cl_2, 125.8 MHz).

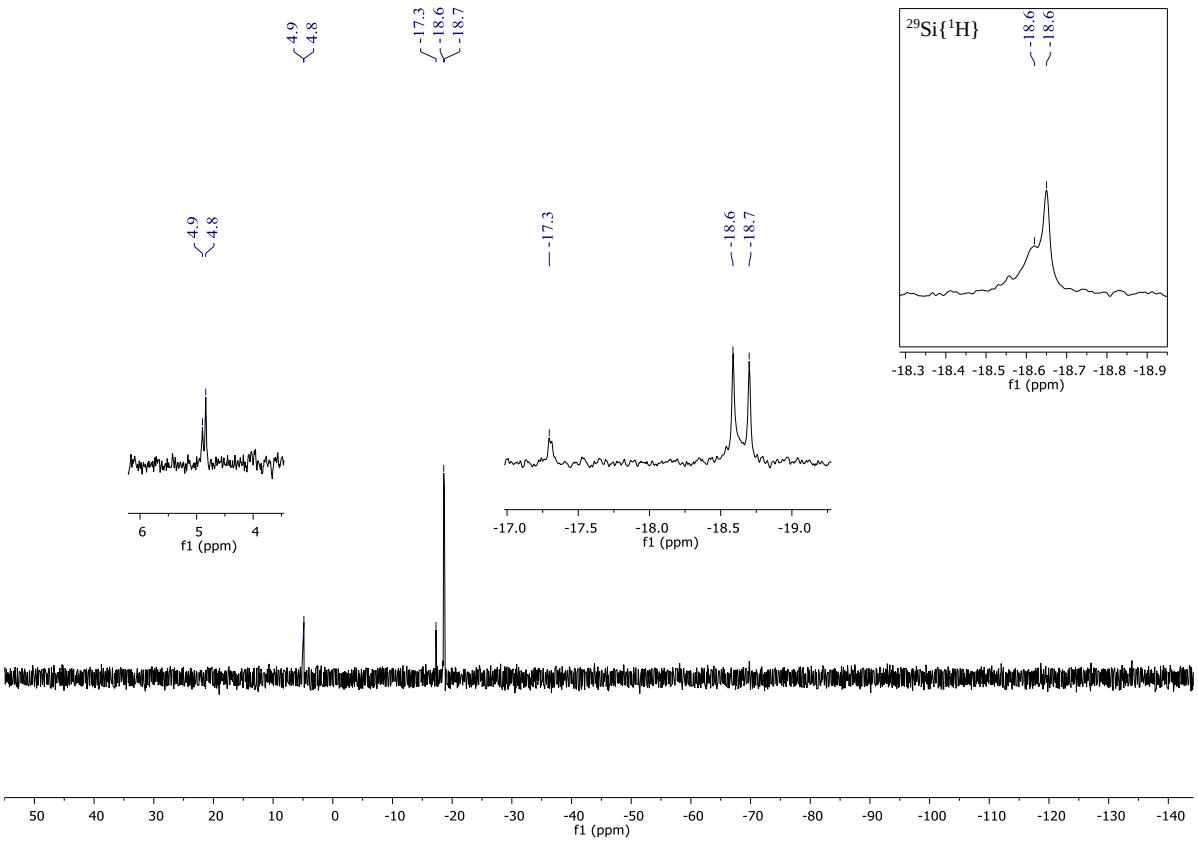

Figure S10: ^{29}Si NMR spectrum of the reaction mixture of **2** with [*n*Bu$_4$N]Cl, which furnishes the monoprotonated species [H**1**]$^-$ (CD_2Cl_2, 99.4 MHz).

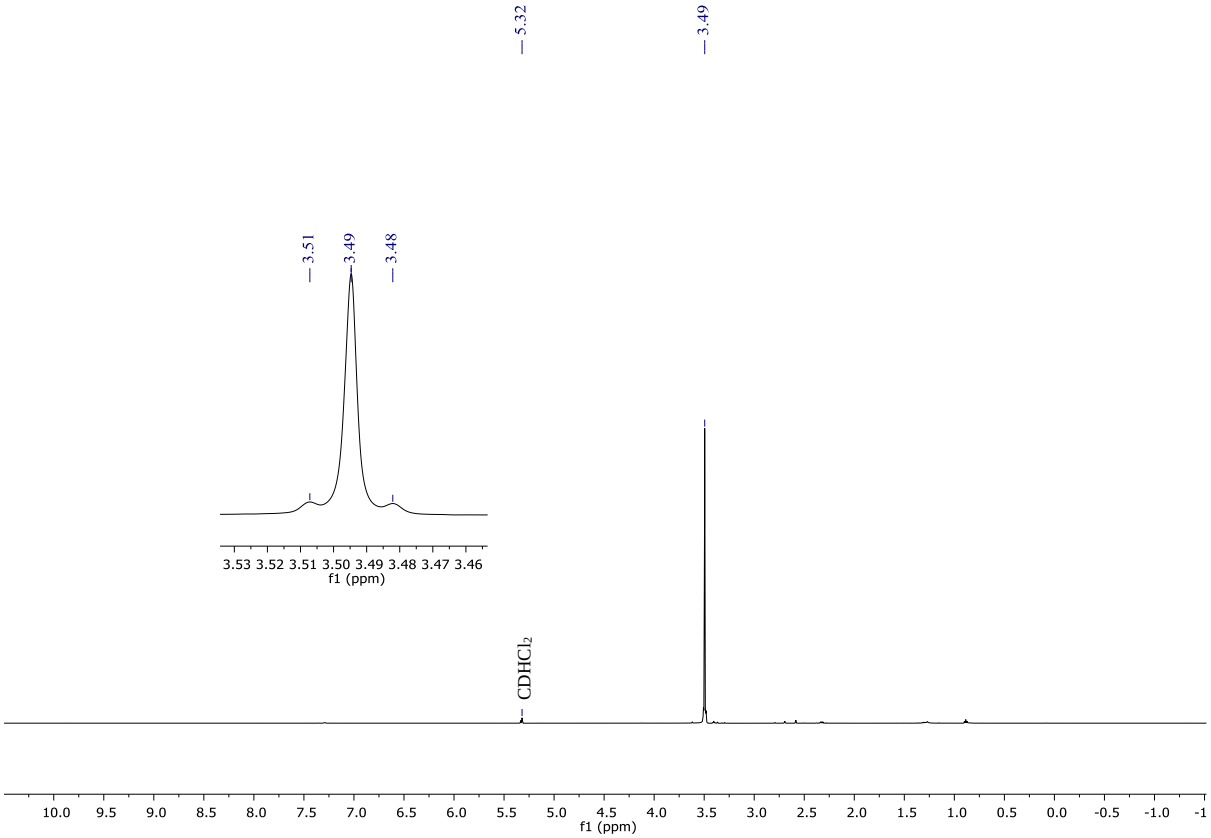

Figure S11: ^{1}H NMR spectrum of **3** (CD_2Cl_2, 500.2 MHz).

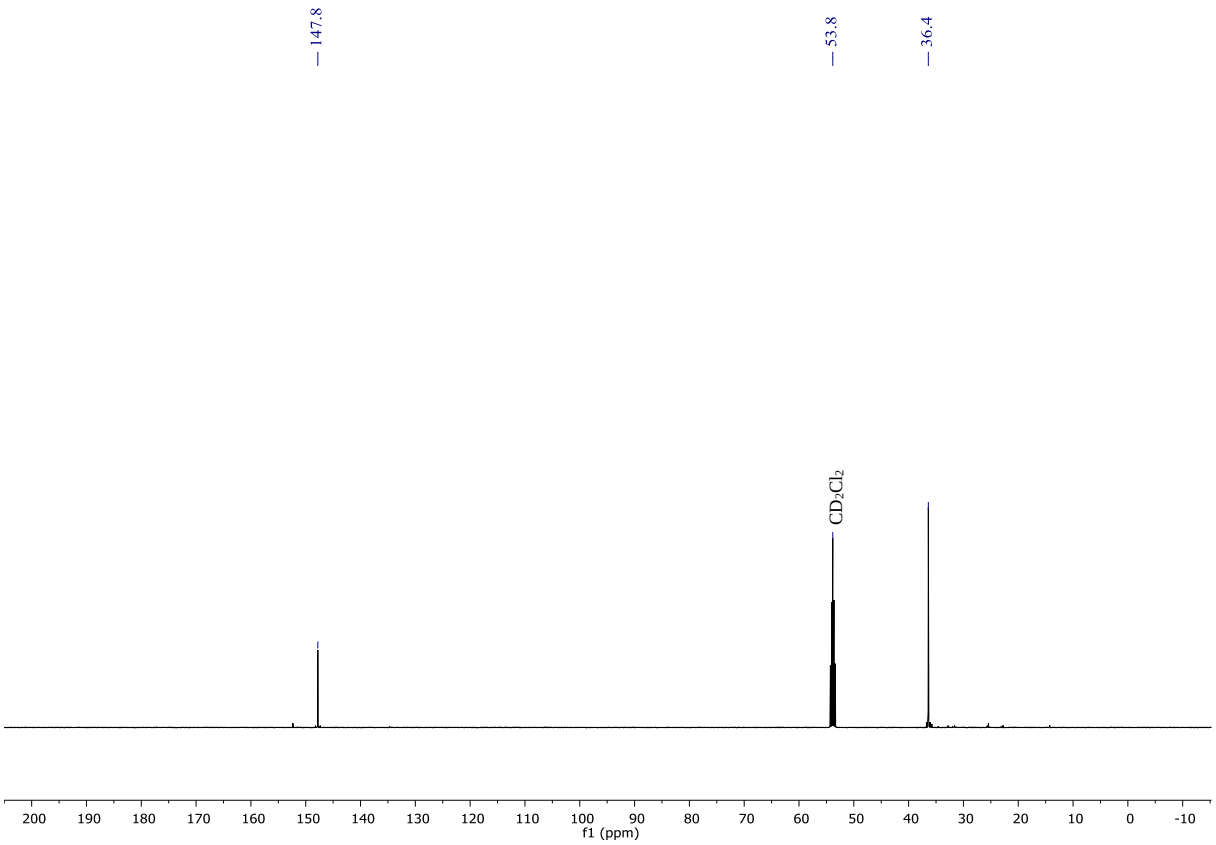

Figure S12: $^{13}C\{^{1}H\}$ NMR spectrum of **3** (CD_2Cl_2, 125.8 MHz).

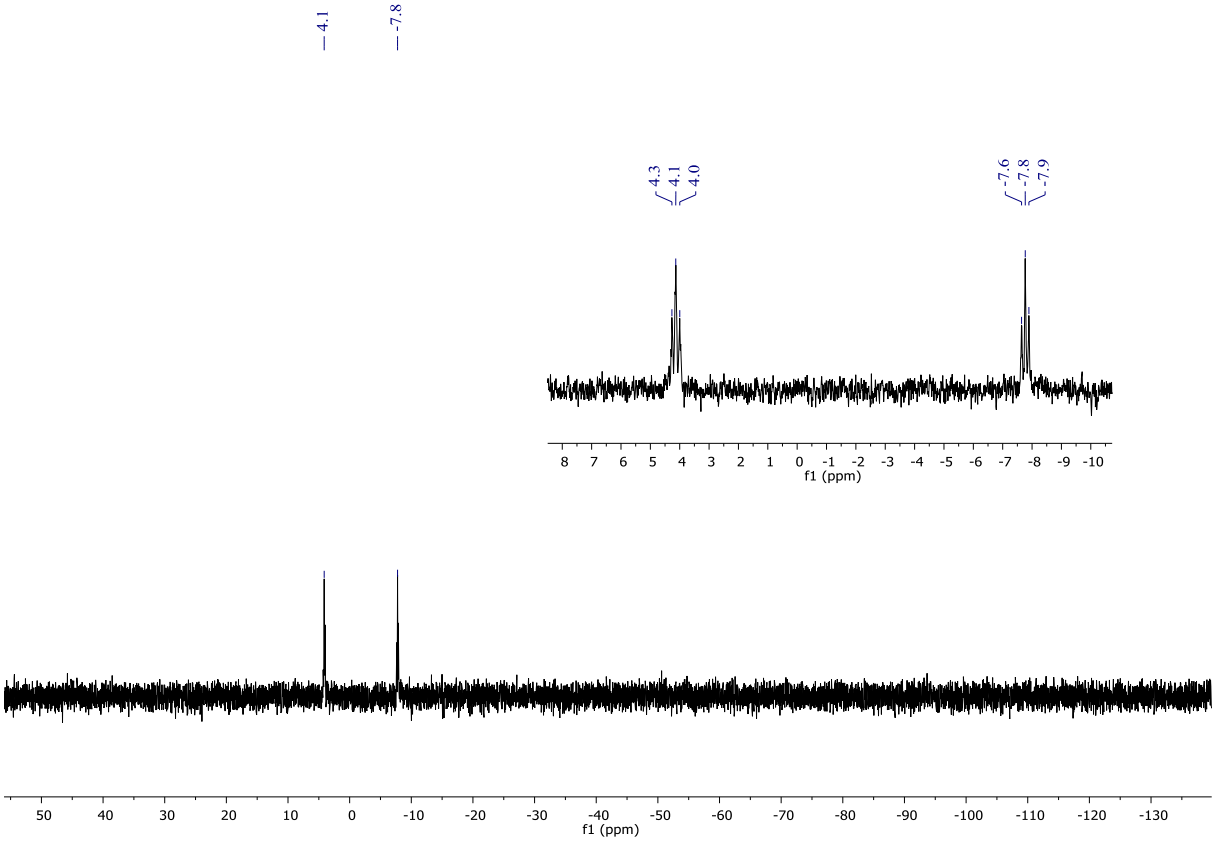

Figure S13: ^{29}Si NMR spectrum of **3** (CD_2Cl_2, 99.4 MHz).

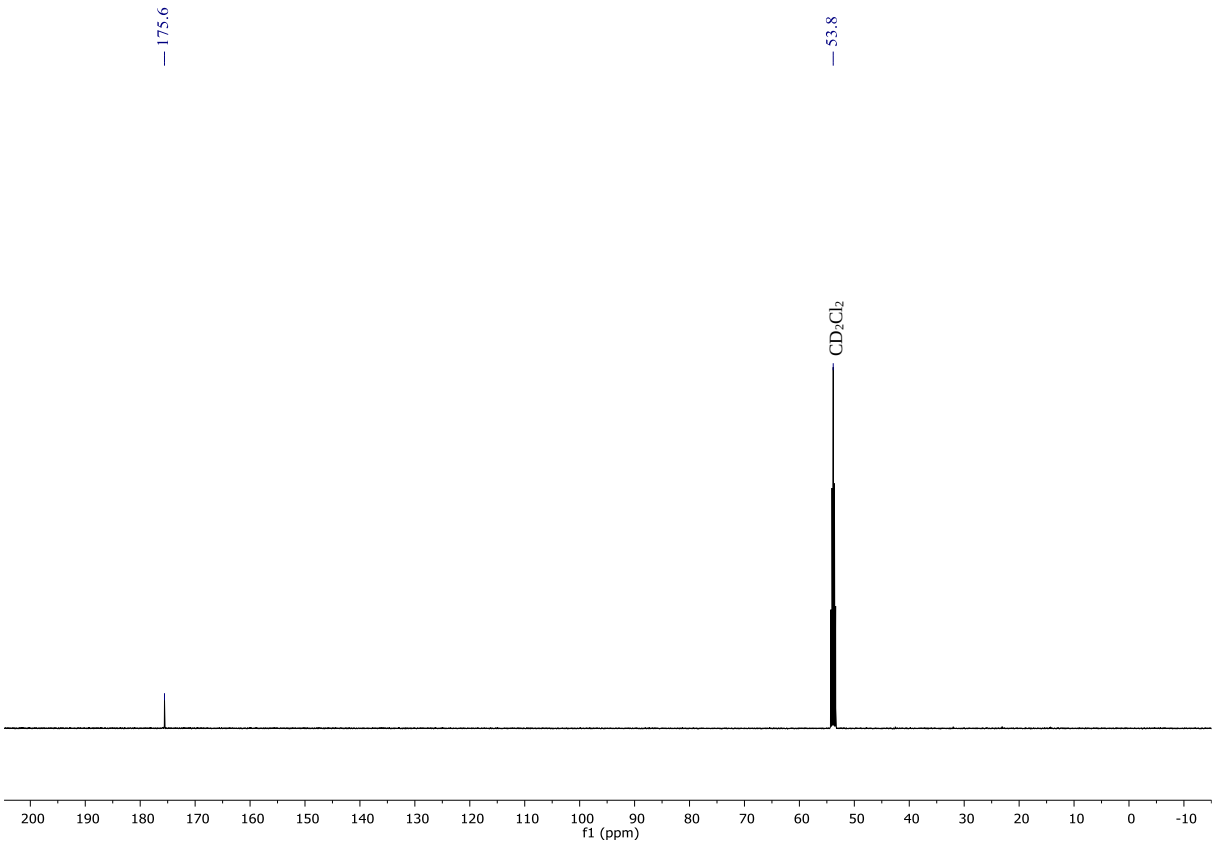

Figure S14: $^{13}C\{^{1}H\}$ NMR spectrum of **4** (CD_2Cl_2, 125.8 MHz, sweep width: –25 ppm to 224 ppm).

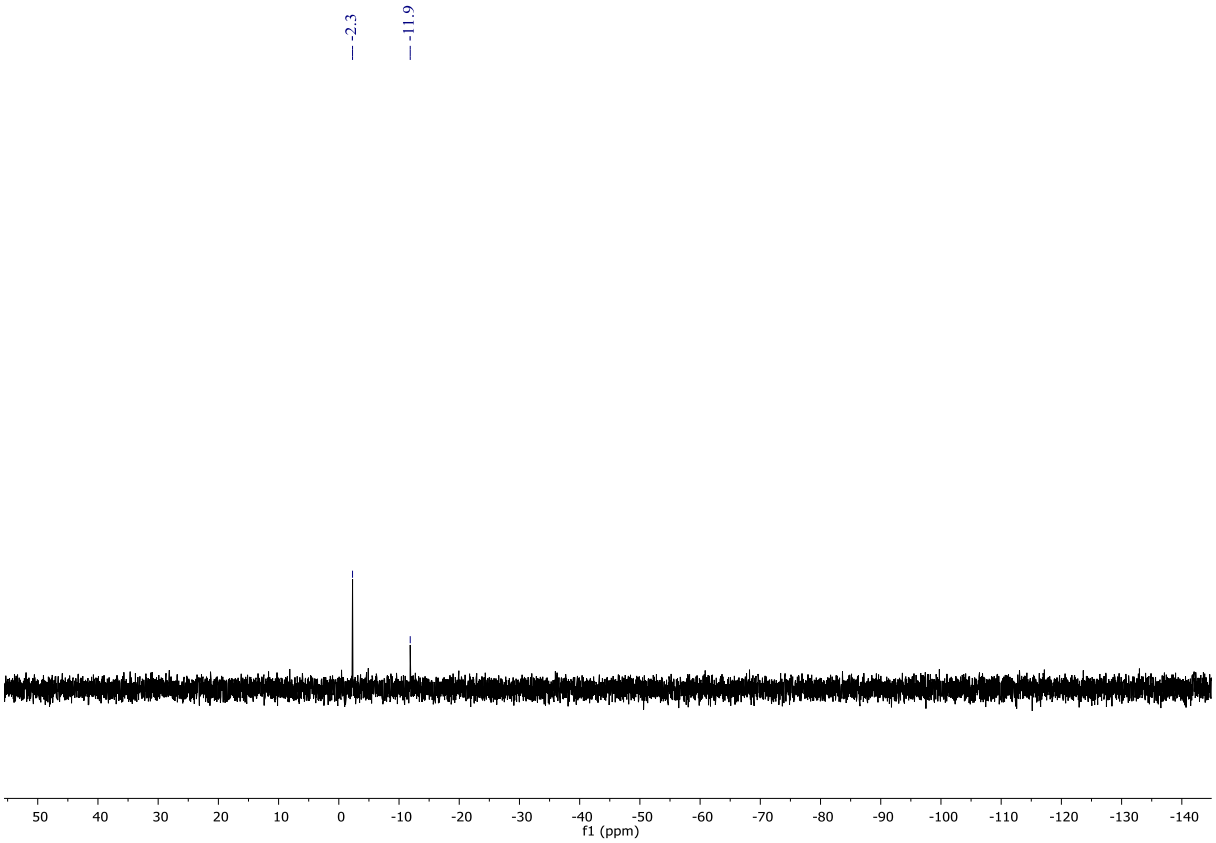

Figure S15: ^{29}Si NMR spectrum of **4** (CD_2Cl_2, 99.4 MHz).

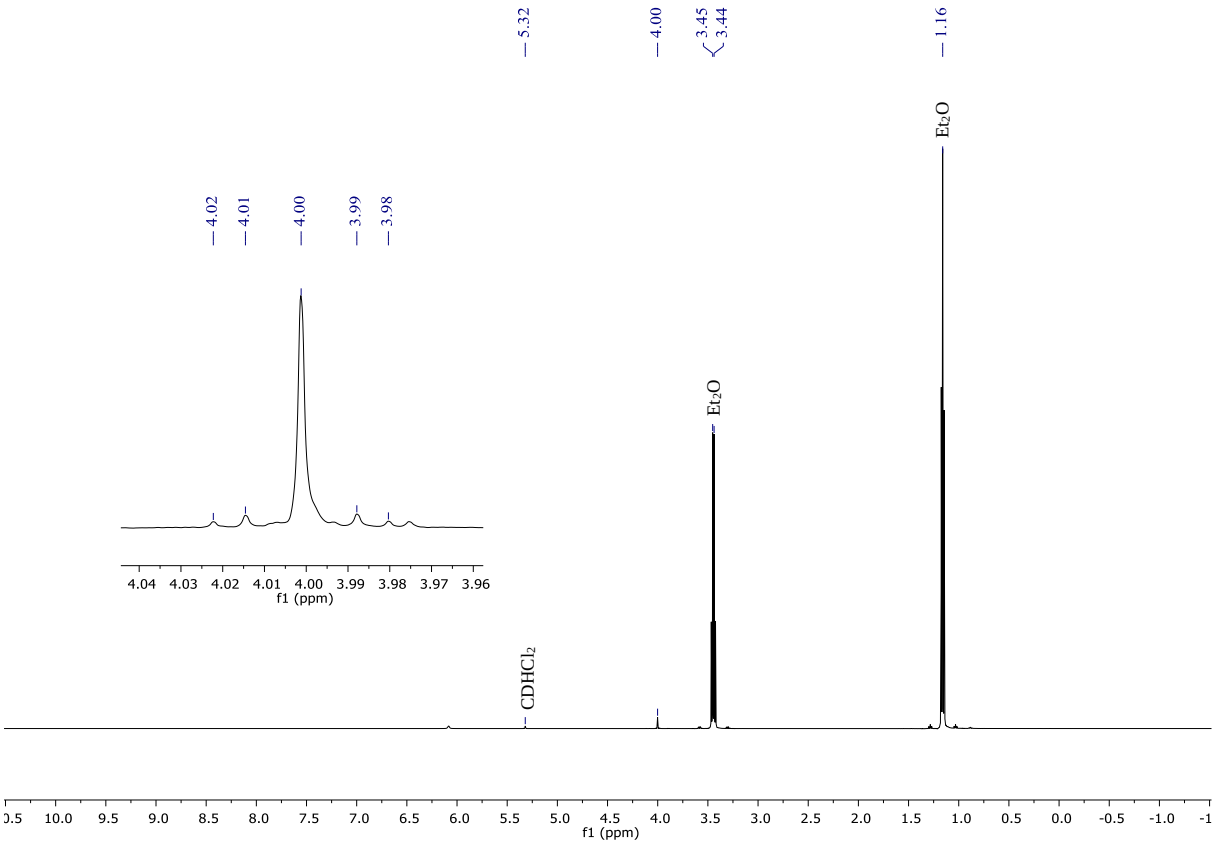

Figure S16: ^{1}H NMR spectrum of the reaction mixture of **4** with HCl, which furnishes **2** (CD_2Cl_2, 500.2 MHz).

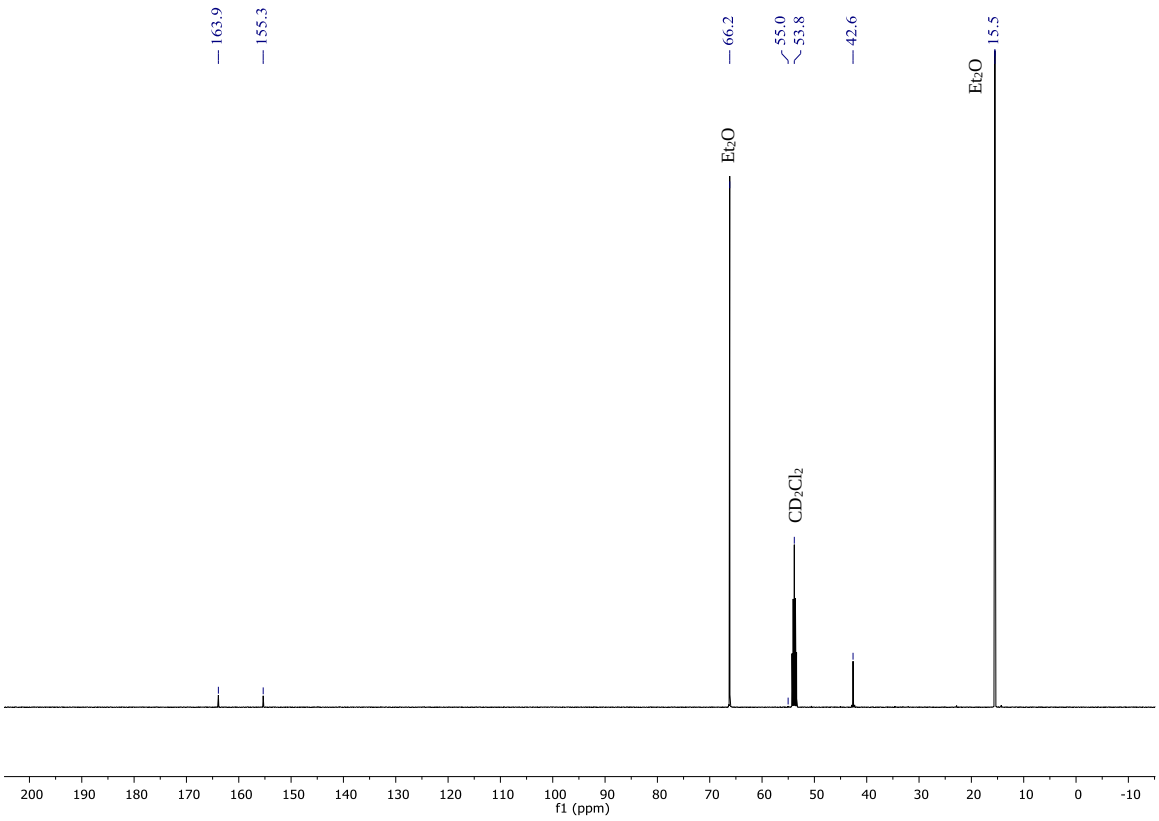

Figure S17: $^{13}C\{^{1}H\}$ NMR spectrum of the reaction mixture of **4** with HCl, which furnishes **2** (CD_2Cl_2, 125.8 MHz).

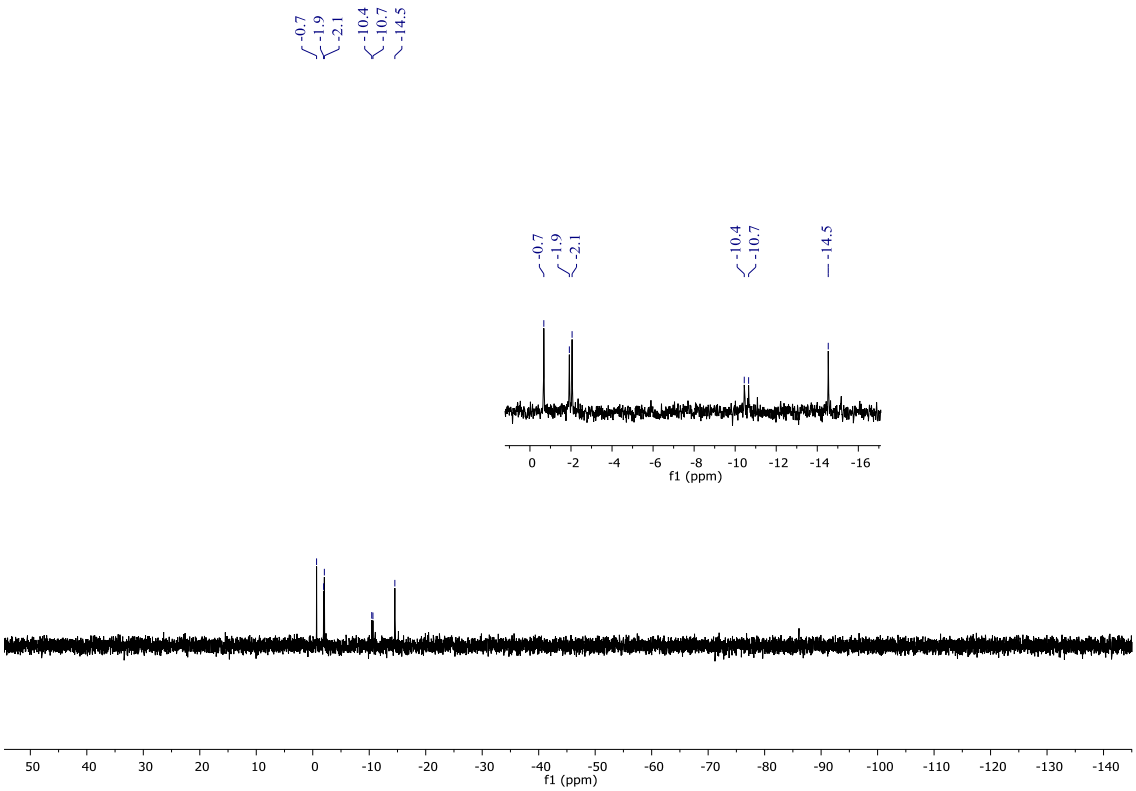

Figure S18: ^{29}Si NMR spectrum of the reaction mixture of **4** with HCl, which furnishes **2** (CD_2Cl_2, 99.4 MHz).

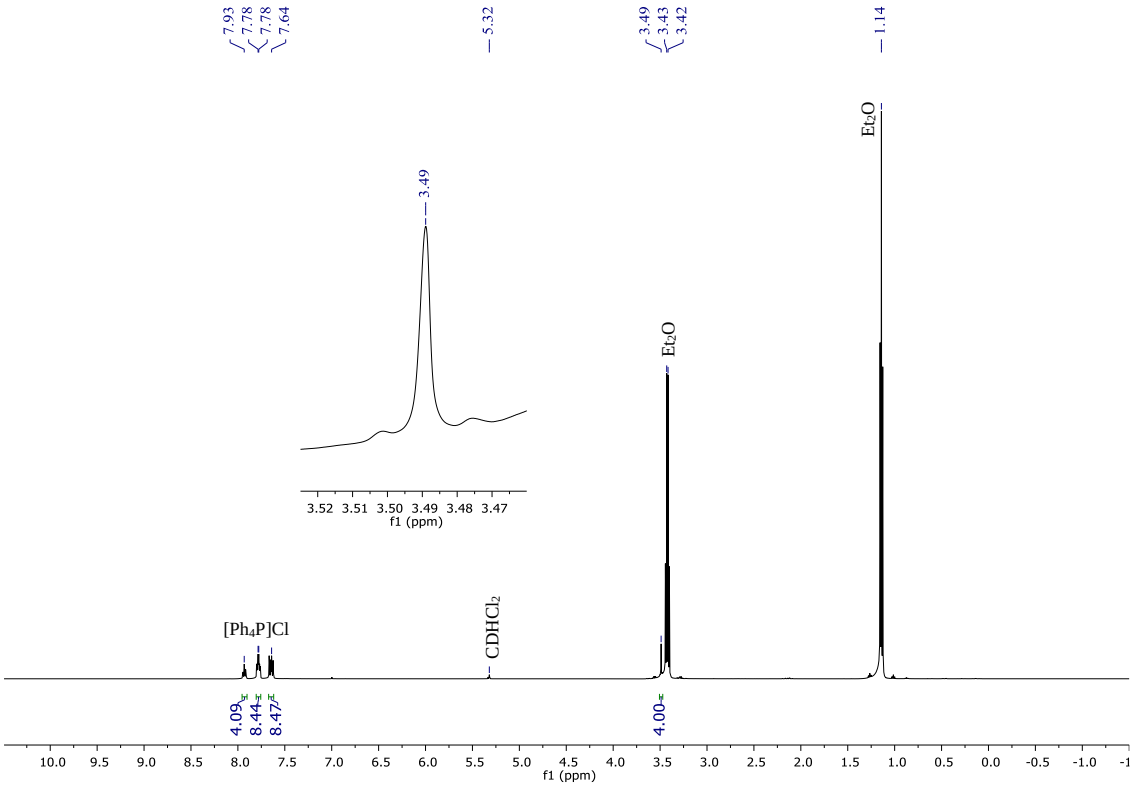

Figure S19: ^{1}H NMR spectrum of the reaction mixture of **2** with $[Ph_4P]Cl$ and HCl, which furnishes **3** (CD_2Cl_2, 500.2 MHz).

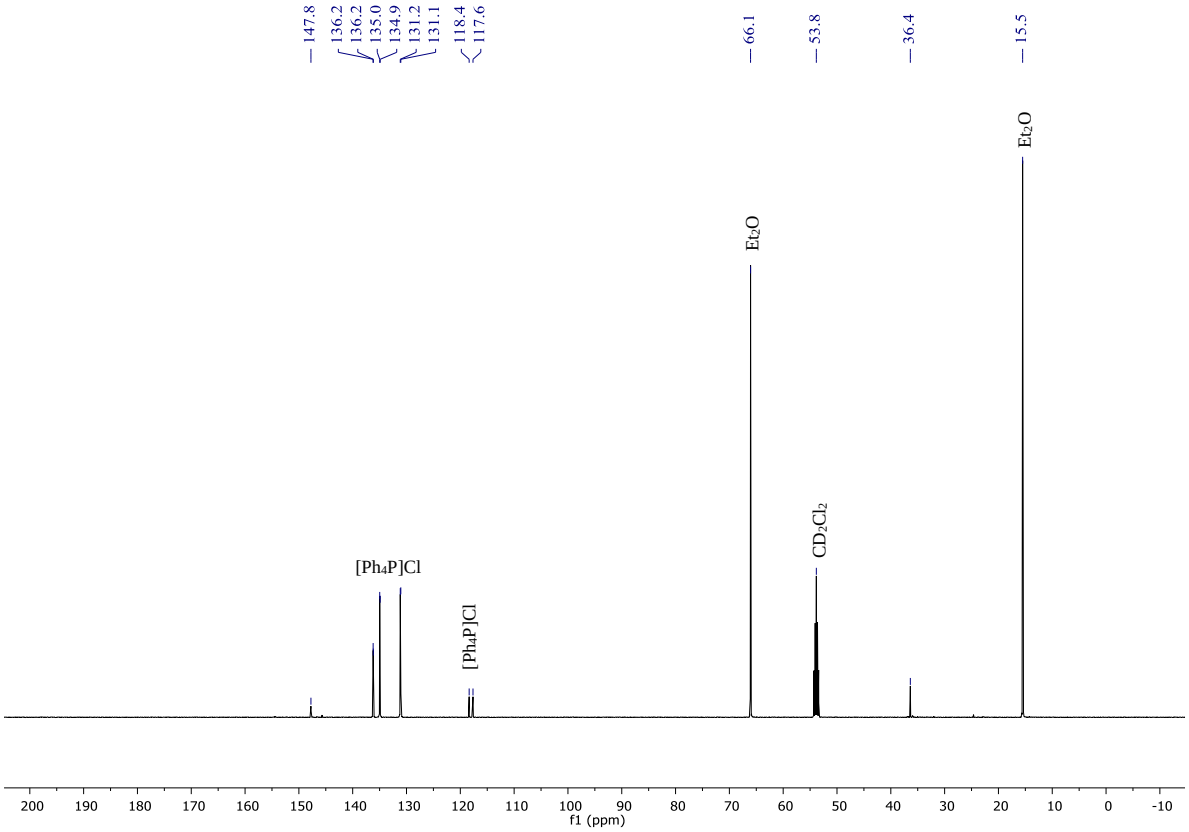

Figure S20: $^{13}C\{^{1}H\}$ NMR spectrum of the reaction mixture of **2** with $[Ph_4P]Cl$ and HCl, which furnishes **3** (CD_2Cl_2, 125.8 MHz).

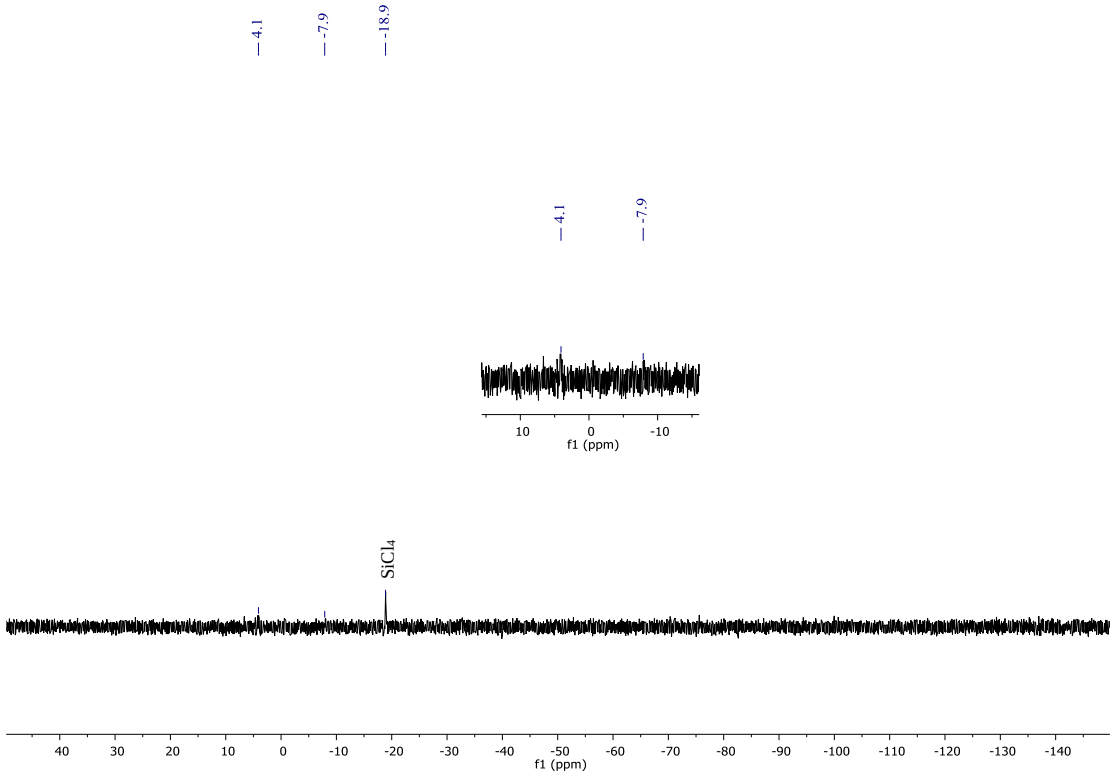

Figure S21: ^{29}Si NMR spectrum of the reaction mixture of **2** with $[Ph_4P]Cl$ and HCl, which furnishes **3** and $SiCl_4$ as a side product(CD_2Cl_2, 99.4 MHz).

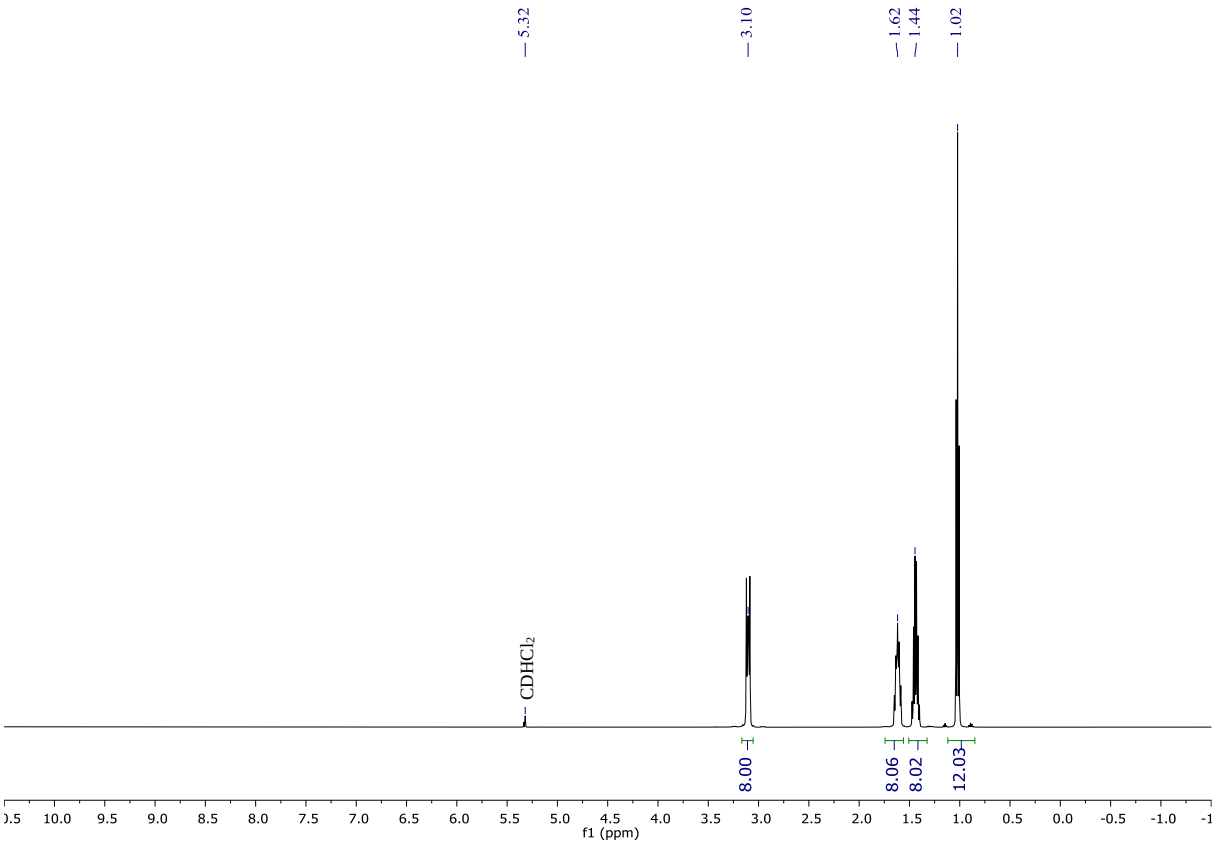

Figure S22: ^{1}H NMR spectrum of the reaction mixture of [**1**]$^{2-}$ with 1 equiv $AlCl_3$, which furnishes [**5**]$^{-}$ (CD_2Cl_2, 500.2 MHz).

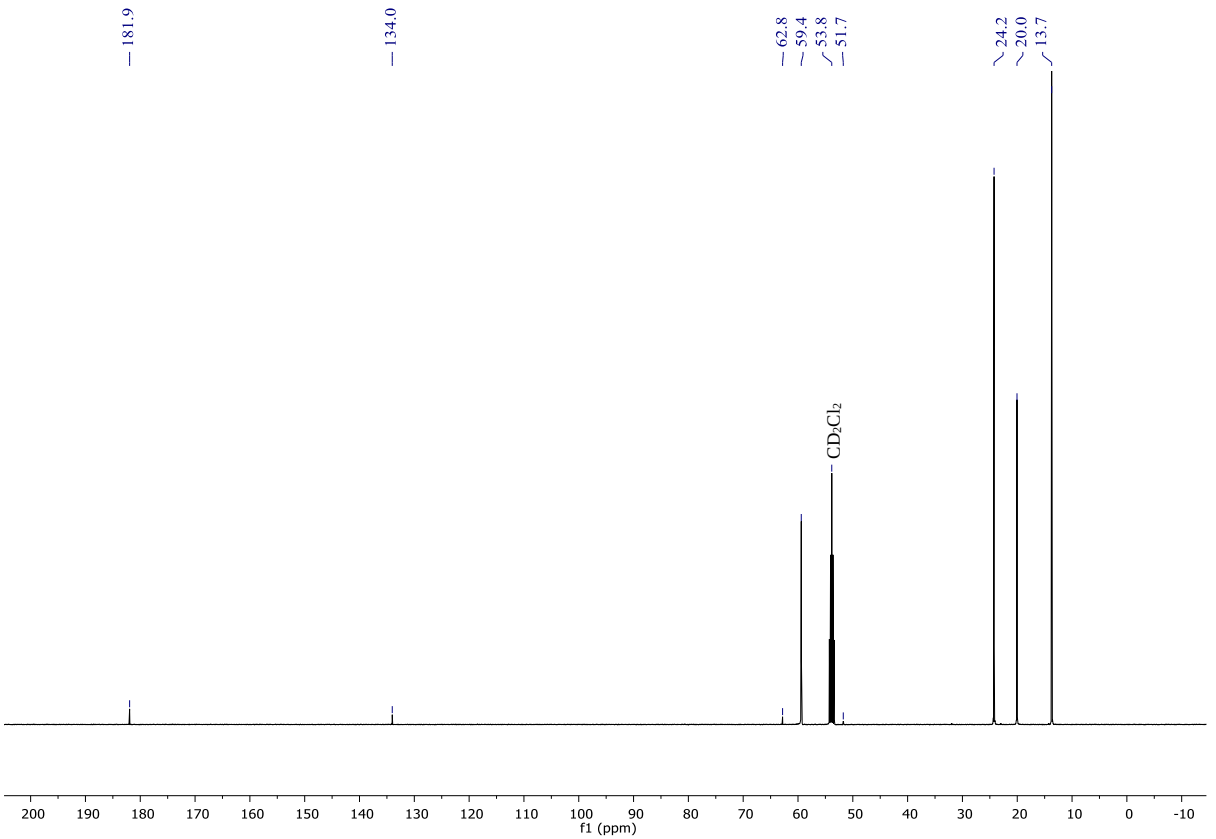

Figure S23: $^{13}C\{^{1}H\}$ NMR spectrum of the reaction mixture of [**1**]$^{2-}$ with 1 equiv $AlCl_3$, which furnishes [**5**]$^{-}$ (CD_2Cl_2, 125.8 MHz).

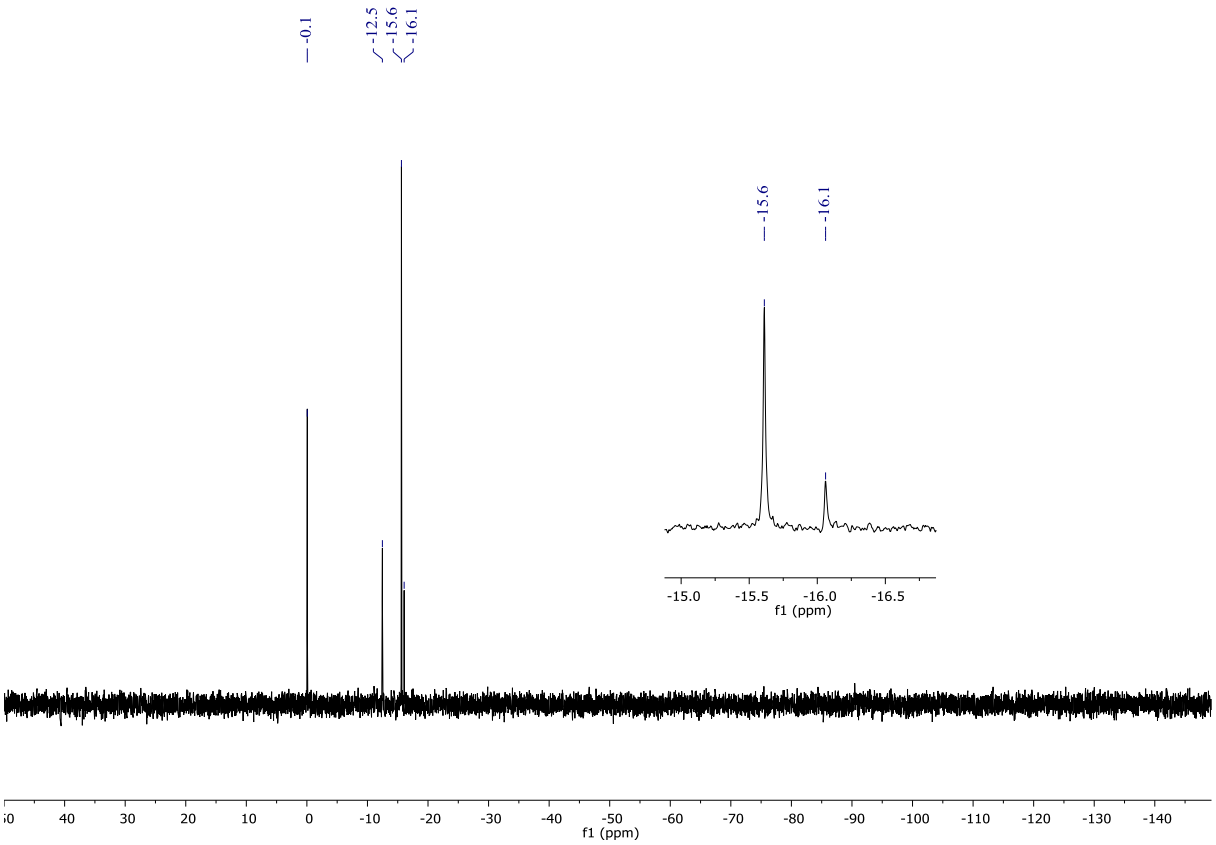

Figure S24: ^{29}Si NMR spectrum of the reaction mixture of [**1**]$^{2-}$ with 1 equiv $AlCl_3$, which furnishes [**5**]$^{-}$ (CD_2Cl_2, 99.4 MHz).

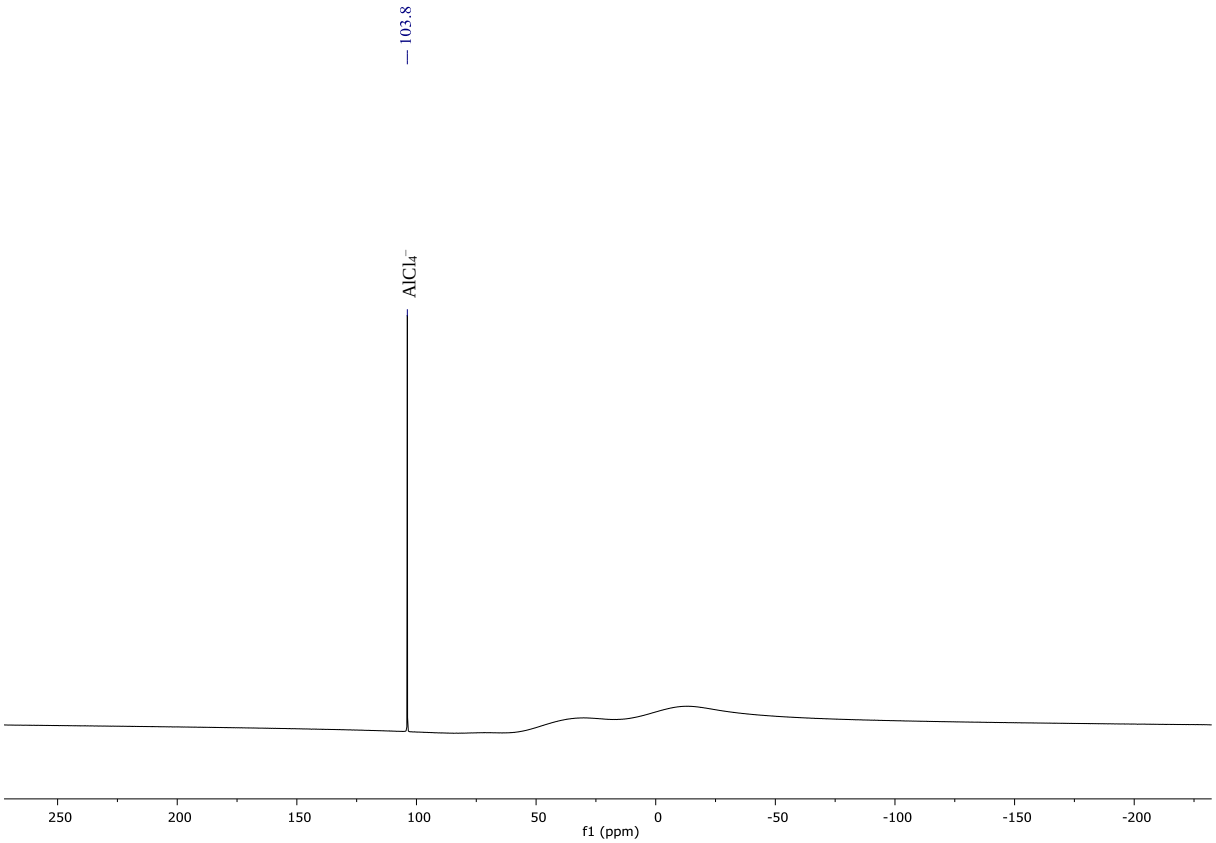

Figure S25: ^{27}Al{^{1}H} NMR spectrum of the reaction mixture of [**1**]$^{2-}$ with 1 equiv $AlCl_3$, which furnishes [**5**]$^{-}$ and $AlCl_4^{-}$ as side product (CD_2Cl_2, 130.3 MHz).

3. X-ray crystal structure analyses

Data for all structures were collected on a STOE IPDS II two-circle diffractometer with a Genix Microfocus tube with mirror optics using MoK_α radiation (λ = 0.71073 Å). The data were scaled using the frame-scaling procedure in the *X-AREA* program system.[S5] The structures were solved by direct methods using the program *SHELXS* and refined against F^2 with full-matrix least-squares techniques using the program *SHELXL*.[S6]

The anion of [*n*Bu$_4$N]$_2$[**1**] is located on a center of inversion. Its central (formal) C=C double bond is disordered over two positions with a site occupation factor of 0.695(18) for the major occupied site.

The dianion of [Ph$_4$P]$_2$[**1**] is located on a center of inversion. The cation is located on a general position. The H atoms were located in a Fourier difference map and refined using a riding model.

Compound **2** crystallizes with two molecules, **2**^{A} and **2**^{B}, in the asymmetric unit. The crystal is twinned with a fractional contribution of 0.583(1) for the major domain. The absolute structure cannot be determined reliably: Flack-x-parameter: 0.48(7). The H atom was located in the difference Fourier map and refined using a riding model.

Compound **3** is located on a center of inversion. The H atoms were located in a Fourier difference map and refined using a riding model.

Compound **4** is located on a center of inversion.

CCDC files CCDC 1999414 ([*n*Bu$_4$N]$_2$[**1**]), CCDC 1999415 ([Ph$_4$P]$_2$[**1**]), CCDC 1999416 (**2**), CCDC 1999417 (**3**), and CCDC 1999418 (**4**) contain the supplementary crystallographic data for this paper and can be obtained free of charge from The Cambridge Crystallographic Data Centre via www.ccdc.cam.ac.uk/data_request/cif.

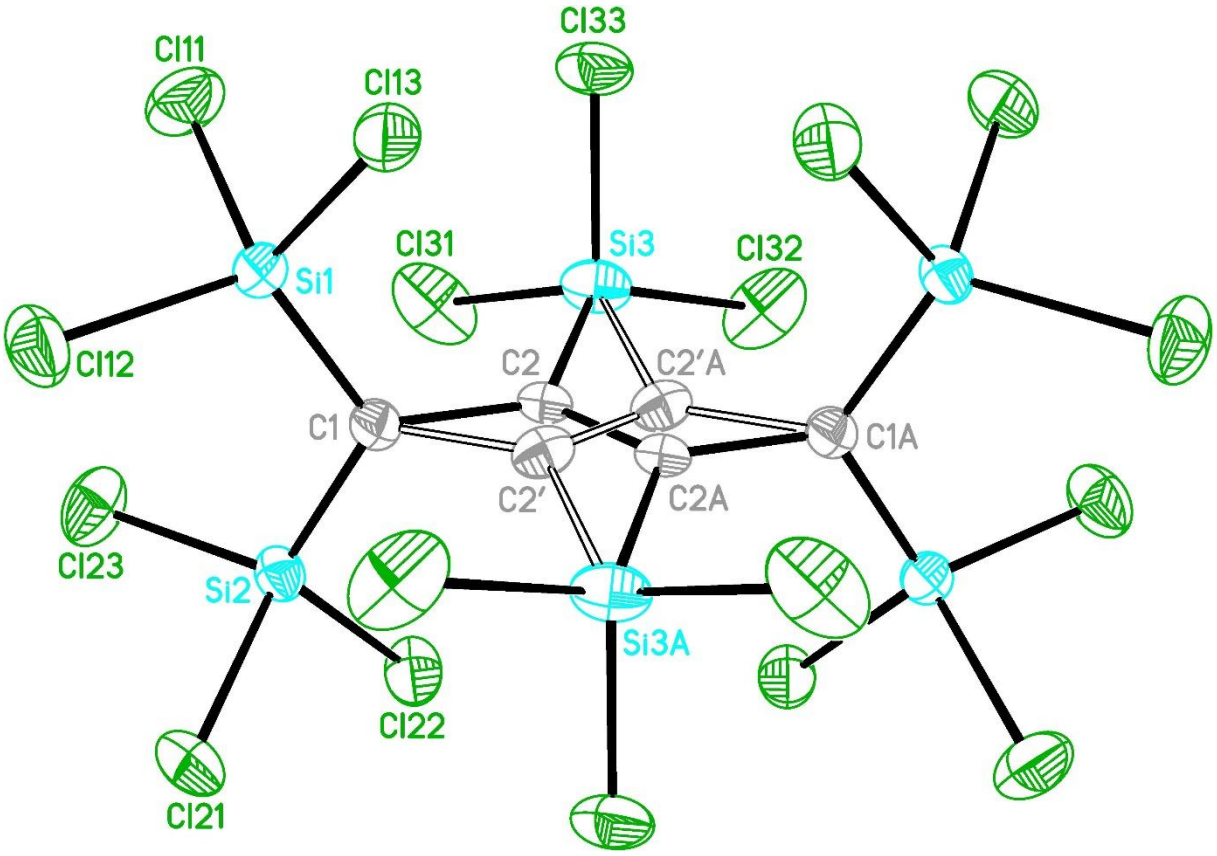

Figure S26: Molecular structure of [*n*Bu$_4$N]$_2$[**1**] in the solid state. Displacement ellipsoids are shown at the 50% probability level. The [*n*Bu$_4$N]$^+$ cations are omitted for clarity. Selected bond lengths [Å], bond angles [°], torsion angles [°], and dihedral angle [°]: C(1)–C(2) = 1.506(5), C(1)–C(2') = 1.53(1), C(2)–C(2A) = 1.36(1), C(2')–C(2'A) = 1.31(3), C(1)–Si(1) = 1.773(3), C(1)–Si(2) = 1.762(3), C(2)–Si(3) = 1.889(6), C(2')–Si(3A) = 1.96(2); C(1)–C(2)–C(2A) = 123.1(7), C(1)–C(2')–C(2'A) = 123(2), C(1)–C(2)–Si(3) = 118.5(4), C(1)–C(2')–Si(3A) = 125.0(9), C(2A)–C(2)–Si(3) = 118.0(5), C(2'A)–C(2)'–Si(3A) = 112(1), C(2)–C(1)–Si(1) = 120.1(2), C(2')–C(1)–Si(1) = 118.1(4), C(2)–C(1)–Si(2) = 119.8(2), C(2')–C(1)–Si(2) = 119.1(4), Si(1)–C(1)–Si(2) = 118.5(2); Si(1)–C(1)–C(2)–C(2A) = 96.5(5), Si(1)–C(1)–C(2')–C(2'A) = –103(1), Si(2)–C(1)–C(2)–C(2A) = –98.2(5), Si(2)–C(1)–C(2')–C(2'A) = 100(1), Si(1)–C(1)–C(2)–Si(3) = –76.5(3), Si(1)–C(1)–C(2')–Si(3A) = 85.0(6), Si(2)–C(1)–C(2)–Si(3) = 88.8(3), Si(2)–C(1)–C(2')–Si(3A) = –71.3(7); Si(1)C(1)Si(2)//C(1)C(2)C(2A)C(1A) = 89.1(3). Symmetry transformation used to generate equivalent atoms: (A) –x, –y+1, –z+1.

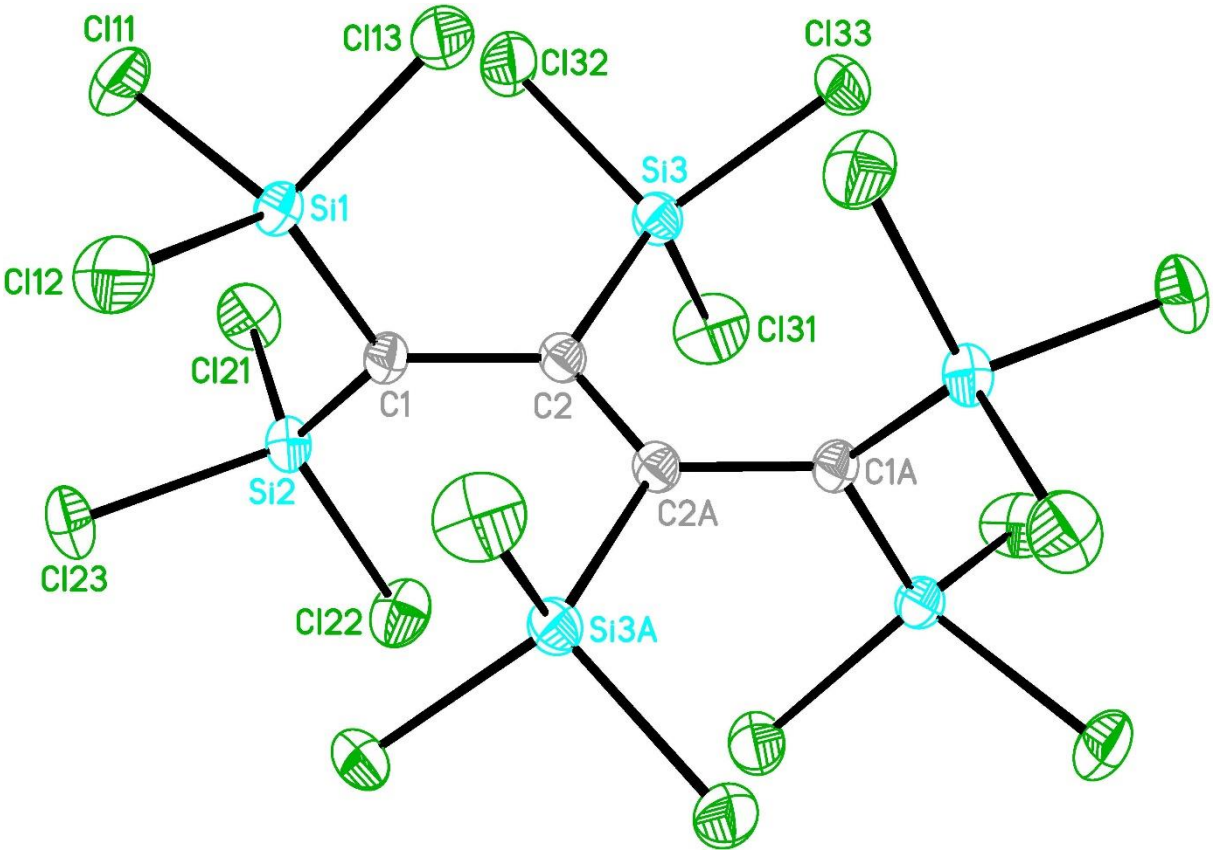

Figure S27: Molecular structure of $[Ph_4P]_2$[**1**] in the solid state. Displacement ellipsoids are shown at the 50% probability level. The $[Ph_4P]^+$ cations are omitted for clarity. Selected bond lengths [Å], bond angles [°], torsion angles [°], and dihedral angle [°]: C(1)–C(2) = 1.501(2), C(2)–C(2A) = 1.353(2), C(1)–Si(1) = 1.774(1), C(1)–Si(2) = 1.777(1), C(2)–Si(3) = 1.882(1); C(1)–C(2)–C(2A) = 123.9(1), C(1)–C(2)–Si(3) = 118.55(9), C(2A)–C(2)–Si(3) = 117.2(1), C(2)–C(1)–Si(1) = 119.11(9), C(2)–C(1)–Si(2) = 119.86(9), Si(1)–C(1)–Si(2) = 117.30(7); Si(1)–C(1)–C(2)–C(2A) = 106.8(2), Si(2)–C(1)–C(2)–C(2A) = –95.6(2), Si(1)–C(1)–C(2)–Si(3) = –79.6(1), Si(2)–C(1)–C(2)–Si(3) = 78.1(1); Si(1)C(1)Si(2)//C(1)C(2)C(2A)C(1A) = 84.6(2). Symmetry transformation used to generate equivalent atoms: (A) –x+1, –y, –z+1.

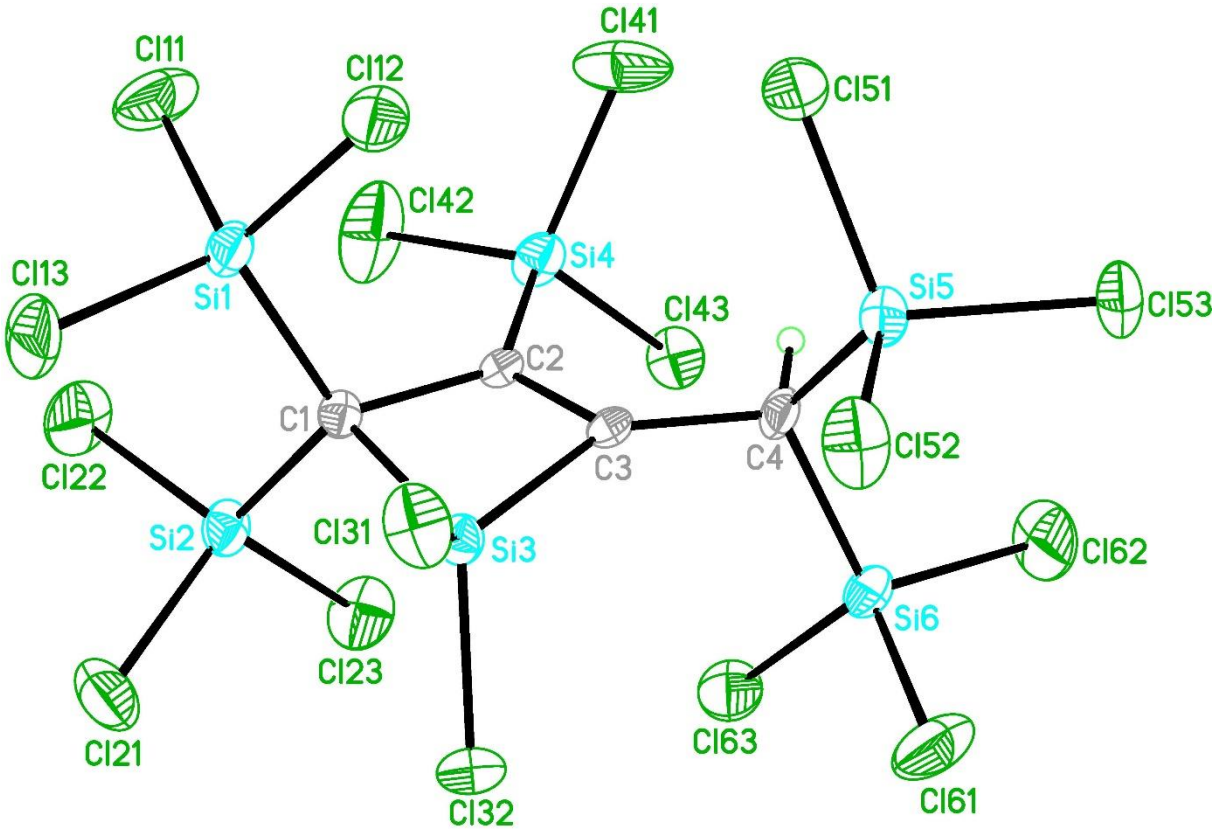

Figure S28: Molecular structure of **2**^{A} in the solid state. Displacement ellipsoids are shown at the 50% probability level. Selected bond lengths [Å], bond angles [°], and torsion angles [°] of **2**^{A}/**2**^{B}: C(1)–C(2) = 1.58(1)/1.57(1), C(2)–C(3) = 1.36(1)/1.36(1), C(3)–C(4) = 1.50(1)/1.51(1), C(1)–Si(1) = 1.884(9)/1.883(9), C(1)–Si(2) = 1.882(9)/1.879(9), C(1)–Si(3) = 1.922(9)/1.92(1), C(2)–Si(4) = 1.872(9)/1.881(9), C(3)–Si(3) = 1.847(9)/1.846(9), C(4)–Si(5) = 1.891(9)/1.894(9), C(4)–Si(6) = 1.887(9)/1.88(1), Si(3)–Cl(31) = 2.024(3)/2.020(4), Si(3)–Cl(32) = 2.027(4)/2.027(3); C(1)–C(2)–C(3) = 108.3(7)/108.1(8), C(2)–C(3)–C(4) = 128.5(8)/128.9(8), C(1)–C(2)–Si(4) = 126.9(6)/126.1(6) , C(1)–Si(3)–C(3) = 78.4(4)/78.2(4), C(2)–C(3)–Si(3) = 90.8(6)/90.7(6), C(2)–C(1)–Si(3) = 81.9(5)/82.2(5), C(4)–C(3)–Si(3) = 140.2(7)/139.9(7), Si(1)–C(1)–Si(2) = 114.4(5)/113.1(5), Si(5)–C(4)–Si(6) = 114.9(5)/115.3(5); C(1)–C(2)–C(3)–C(4) = – 179.3(8)/179.0(8), C(1)–C(2)–C(3)–Si(3) = 6.9(7)/–8.1(7), Si(1)–C(1)–C(2)–C(3) = 104.6(7)/118.7(7), Si(2)–C(1)–C(2)–C(3) = –118.5(7)/–104.9(7), Si(3)–C(1)–C(2)–Si(4) = 173.5(6)/–174.2(6), C(2)–C(3)–C(4)–Si(5) = 120.4(9)/108.9(9), C(2)–C(3)–C(4)–Si(6) = –108.5(9)/–119.8(9).

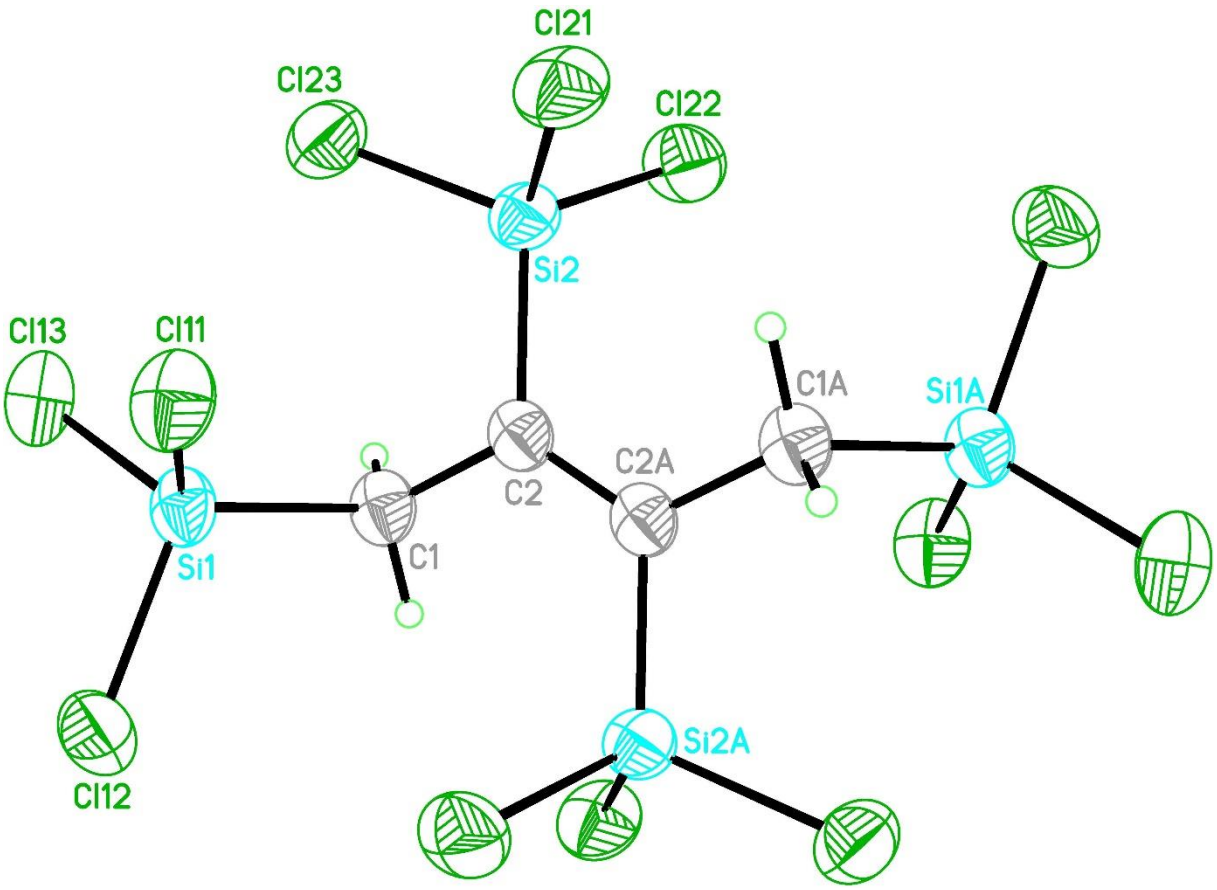

Figure S29: Molecular structure of **3** in the solid state. Displacement ellipsoids are shown at the 50% probability level. Selected bond lengths [Å], bond angles [°], and torsion angles [°]: C(1)–C(2) = 1.532(8), C(2)–C(2A) = 1.35(1), C(1)–Si(1) = 1.869(6), C(2)–Si(2) = 1.881(6); C(1)–C(2)–C(2A) = 123.6(7), C(1)–C(2)–Si(2) = 114.7(4), C(2)–C(1)–Si(1) = 118.7(4), C(2A)–C(2)–Si(2) = 121.5(6); Si(1)–C(1)–C(2)–C(2A) = 109.4(7), Si(1)–C(1)–C(2)–Si(2) = –76.6(5). Symmetry transformation used to generate equivalent atoms: (A) –x+1, –y+1, –z+1.

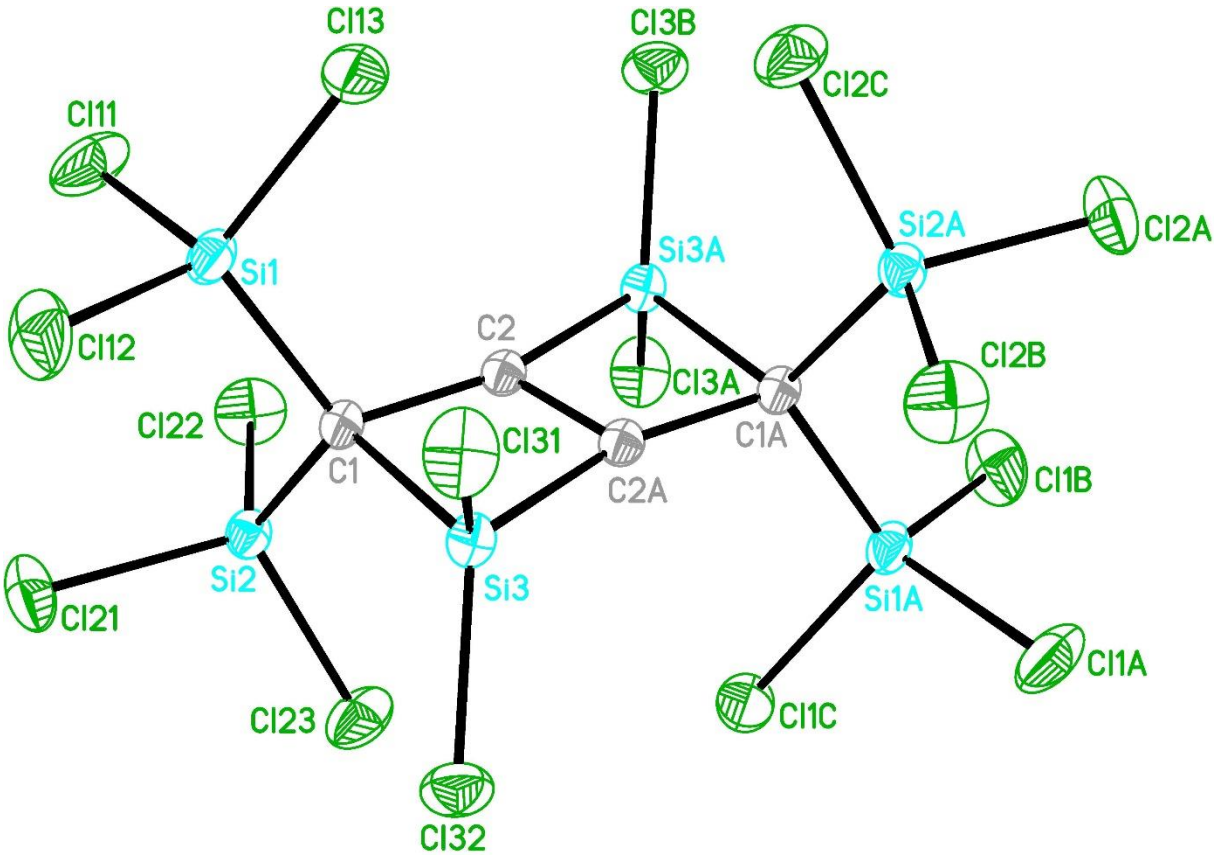

Figure S30: Molecular structure of **4** in the solid state. Displacement ellipsoids are shown at the 50% probability level. Selected bond lengths [Å], bond angles [°], and torsion angles [°]: C(1)–C(2) = 1.538(2), C(2)–C(2A) = 1.366(3), C(1)–Si(1) = 1.881(1), C(1)–Si(2) = 1.878(2), C(1)–Si(3) = 1.943(1), C(2)–Si(3A) = 1.841(2); C(1)–C(2)–C(2A) = 110.8(2), C(1)–C(2)–Si(3A) = 159.3(1), C(1)–Si(3)–C(2A) = 78.38(6), C(2A)–C(2)–Si(3A) = 89.6(1), C(2)–C(1)–Si(1) = 114.1(1), C(2)–C(1)–Si(2) = 110.32(9), C(2)–C(1)–Si(3) = 81.10(8), Si(1)–C(1)–Si(2) = 112.90(7), Si(1)–C(1)–Si(3) = 114.87(7), Si(2)–C(1)–Si(3) = 119.53(7); C(1)–C(2)–C(2A)–Si(3) = –3.7(2) , Si(1)–C(1)–C(2)–C(2A) = 116.9(2), Si(2)–C(1)–C(2)–C(2A) = –114.7(2). Symmetry transformation used to generate equivalent atoms: (A) –x+1, –y+1, –z+2.

Table S1. Crystal data and structure refinement for [*n*Bu_4N]$_2$[**1**].

Identification code	wa2765	
Empirical formula	C_{36} H_{72} Cl_{18} N_2 Si_6	
Formula weight	1339.59	
Temperature	173(2) K	
Wavelength	0.71073 Å	
Crystal system	Monoclinic	
Space group	$P2_1/n$ (No. 14)	
Unit cell dimensions	a = 11.9611(5) Å	α = 90°
	b = 13.7565(4) Å	β = 91.043(3)°
	c = 19.0792(8) Å	γ = 90°
Volume	3138.8(2) Å^3	
Z	2	
Density (calculated)	1.417 Mg/m^3	
Absorption coefficient	0.928 mm^{-1}	
F(000)	1384	
Crystal size	0.280 x 0.160 x 0.150 mm^3	
Theta range for data collection	3.407 to 27.712°	
Index ranges	–15<=h<=15, –17<=k<=17, –24<=l<=24	
Reflections collected	55613	
Independent reflections	7241 [R(int) = 0.0531]	
Completeness to theta = 25.000°	99.8%	
Absorption correction	Semi-empirical from equivalents	
Max. and min. transmission	1.000 and 0.600	
Refinement method	Full-matrix least-squares on F^2	
Data / restraints / parameters	7241 / 0 / 290	
Goodness-of-fit on F^2	1.269	
Final R indices [I>2sigma(I)]	R_1 = 0.0562, wR_2 = 0.0958	
R indices (all data)	R_1 = 0.0695, wR_2 = 0.0996	
Largest diff. peak and hole	0.449 and –0.613 e Å^{-3}	

Table S2. Crystal data and structure refinement for $[Ph_4P]_2$[**1**].

Identification code	wa2915	
Empirical formula	$C_{52}\ H_{40}\ Cl_{18}\ P_2\ Si_6$	
Formula weight	1533.42	
Temperature	173(2) K	
Wavelength	0.71073 Å	
Crystal system	Triclinic	
Space group	*P* -1	
Unit cell dimensions	*a* = 11.4940(4) Å	α = 88.055(3)°
	b = 12.5358(5) Å	β = 64.638(3)°
	c = 12.9082(5) Å	γ = 74.620(3)°
Volume	1613.7(1) $Å^3$	
Z	1	
Density (calculated)	1.578 Mg/m^3	
Absorption coefficient	0.961 mm^{-1}	
F(000)	772	
Crystal size	0.230 x 0.140 x 0.080 mm^3	
Theta range for data collection	3.200 to 27.617°	
Index ranges	–14<=h<=14, –16<=k<=16, –16<=l<=16	
Reflections collected	36606	
Independent reflections	7401 [*R*(int) = 0.0228]	
Completeness to theta = 25.000°	99.8 %	
Absorption correction	Semi-empirical from equivalents	
Max. and min. transmission	1.000 and 0.674	
Refinement method	Full-matrix least-squares on F^2	
Data / restraints / parameters	7401 / 0 / 352	
Goodness-of-fit on F^2	1.040	
Final *R* indices [I>2sigma(I)]	R_1 = 0.0246, wR_2 = 0.0642	
R indices (all data)	R_1 = 0.0281, wR_2 = 0.0665	
Largest diff. peak and hole	0.352 and –0.372 e $Å^{-3}$	

Table S3. Crystal data and structure refinement for **2**.

Identification code	wa2879	
Empirical formula	C_4 H Cl_{17} Si_6	
Formula weight	820.24	
Temperature	173(2) K	
Wavelength	0.71073 Å	
Crystal system	Triclinic	
Space group	*P* 1 (No. 1)	
Unit cell dimensions	*a* = 8.7877(7) Å	α = 77.830(6)°
	b = 9.1419(7) Å	β = 89.935(6)°
	c = 19.022 (2) Å	γ = 66.457(6)°
Volume	1363.6(2) $Å^3$	
Z	2	
Density (calculated)	1.998 Mg/m^3	
Absorption coefficient	1.970 mm^{-1}	
F(000)	796	
Crystal size	0.160 x 0.110 x 0.040 mm^3	
Theta range for data collection	3.203 to 25.918°	
Index ranges	–10<=h<=10, –11<=k<=11, –23<=l<=23	
Reflections collected	27689	
Independent reflections	27689 [*R*(int) = ?]	
Completeness to theta = 25.000°	99.6 %	
Absorption correction	Semi-empirical from equivalents	
Max. and min. transmission	1.000 and 0.618	
Refinement method	Full-matrix least-squares on F^2	
Data / restraints / parameters	27689 / 3 / 488	
Goodness-of-fit on F^2	1.019	
Final *R* indices [I>2sigma(I)]	R_1 = 0.0470, wR_2 = 0.1228	
R indices (all data)	R_1 = 0.0510, wR_2 = 0.1274	
Absolute structure parameter	0.48(7)	
Largest diff. peak and hole	0.615 and –0.423 e $Å^{-3}$	

Table S4. Crystal data and structure refinement for **3**.

Identification code	wa2911	
Empirical formula	$C_4 H_4 Cl_{12} Si_4$	
Formula weight	589.83	
Temperature	173(2) K	
Wavelength	0.71073 Å	
Crystal system	Triclinic	
Space group	*P* -1	
Unit cell dimensions	*a* = 6.9328(8) Å	α = 118.304(8)°
	b = 9.038 (1) Å	β = 90.993(9)°
	c = 9.304(1) Å	γ = 102.669(9)°
Volume	495.7 (1) $Å^3$	
Z	1	
Density (calculated)	1.976 Mg/m^3	
Absorption coefficient	1.901 mm^{-1}	
F(000)	288	
Crystal size	0.150 x 0.130 x 0.020 mm^3	
Theta range for data collection	3.480 to 25.015°	
Index ranges	–8<=h<=8, –10<=k<=10, –11<=l<=10	
Reflections collected	8475	
Independent reflections	1746 [*R*(int) = 0.0606]	
Completeness to theta = 25.000°	99.7 %	
Absorption correction	Semi-empirical from equivalents	
Max. and min. transmission	1.000 and 0.718	
Refinement method	Full-matrix least-squares on F^2	
Data / restraints / parameters	1746 / 0 / 91	
Goodness-of-fit on F^2	1.137	
Final *R* indices [I>2sigma(I)]	R_1 = 0.0688, wR_2 = 0.1733	
R indices (all data)	R_1 = 0.0796, wR_2 = 0.1815	
Largest diff. peak and hole	0.796 and –0.632 e $Å^{-3}$	

Table S5. Crystal data and structure refinement for **4**.

Identification code	wa2874	
Empirical formula	$C_4 Cl_{16} Si_6$	
Formula weight	783.78	
Temperature	173(2) K	
Wavelength	0.71073 Å	
Crystal system	Triclinic	
Space group	*P* -1 (No. 2)	
Unit cell dimensions	*a* = 8.6694(5) Å	α = 92.531(5)°
	b = 8.9026(6) Å	β = 104.748(5)°
	c = 9.9167(6) Å	γ = 116.156(5)°
Volume	653.49(8) $Å^3$	
Z	1	
Density (calculated)	1.992 Mg/m^3	
Absorption coefficient	1.952 mm^{-1}	
F(000)	380	
Crystal size	0.150 x 0.130 x 0.120 mm^3	
Theta range for data collection	3.265 to 27.535°	
Index ranges	–11<=h<=11, –11<=k<=10, –12<=l<=12	
Reflections collected	12629	
Independent reflections	2984 [*R*(int) = 0.0268]	
Completeness to theta = 25.000°	99.5 %	
Absorption correction	Semi-empirical from equivalents	
Max. and min. transmission	1.000 and 0.553	
Refinement method	Full-matrix least-squares on F^2	
Data / restraints / parameters	2984 / 0 / 119	
Goodness-of-fit on F^2	1.095	
Final *R* indices [I>2sigma(I)]	R_1 = 0.0226, wR_2 = 0.0573	
R indices (all data)	R_1 = 0.0247, wR_2 = 0.0589	
Extinction coefficient	0.020(2)	
Largest diff. peak and hole	0.507 and –0.370 e $Å^{-3}$	

4. Differential thermal analysis and thermogravimetry (DTA/TG) of 2, 3, and 4

Differential thermal and thermogravimetric analysis (DTA/TG) were performed on a SETARAM (TGA 92) device. The sample was placed in an Al_2O_3 crucible and heated under Ar atmosphere with a heating rate of 10 K/min and a constant Ar flow rate of about 75 mL/min.

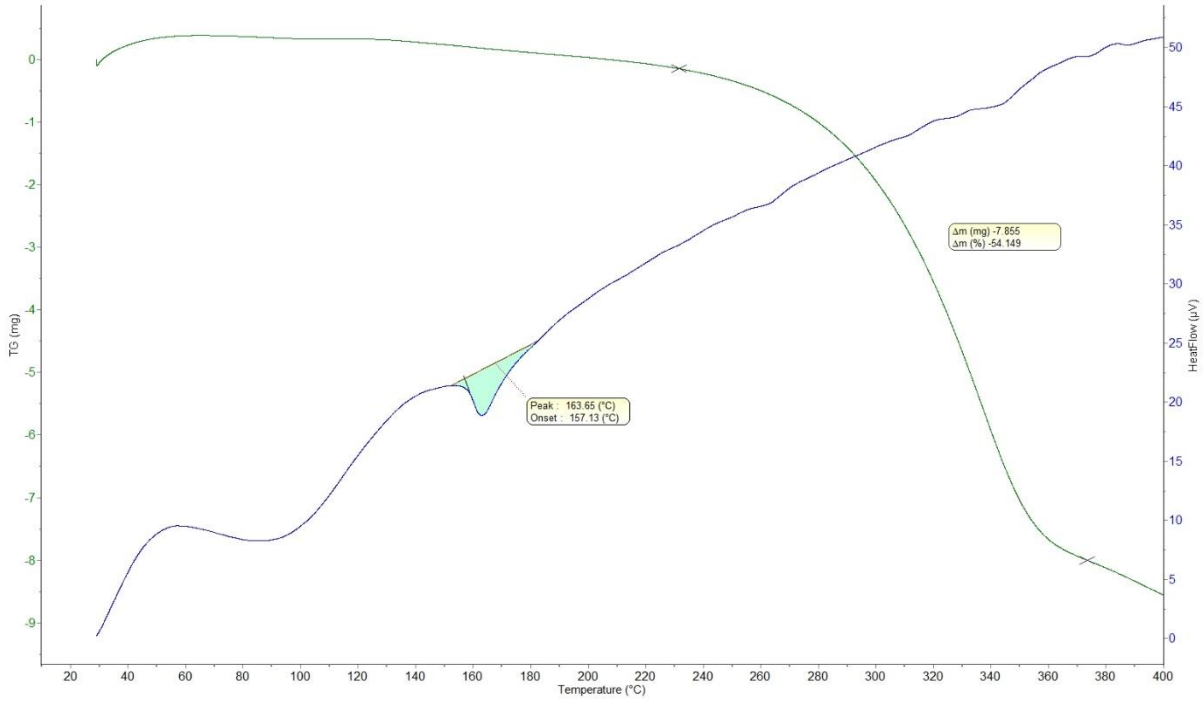

Figure S31: DTA/TG curve of **2**; the endothermic event between 60 and 120 °C is a known artifact of the apparatus used for the measurement. Decomposition of **2** starts at 230 °C with an overall mass loss of 54%.

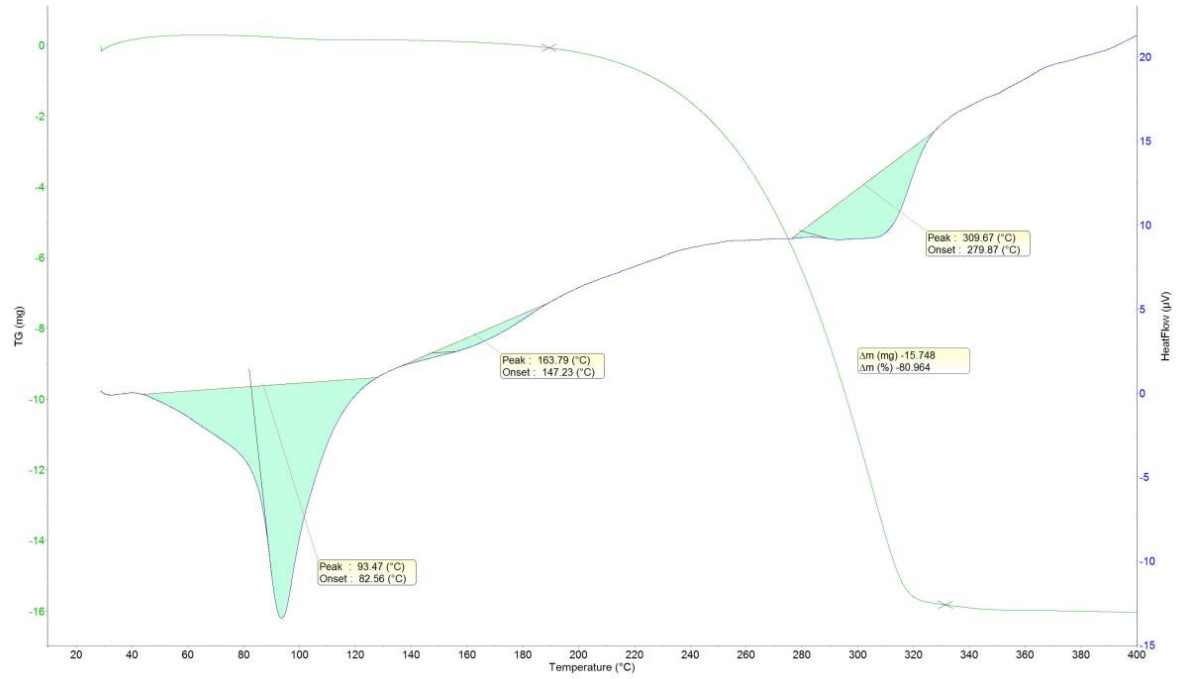

Figure S32: DTA/TG curve of **3**; the endothermic event between 80 and 120 °C corresponds to the melting point of **3** (mp = 87.6 °C). Decomposition of **3** starts at 190 °C with an overall mass loss of 81%.

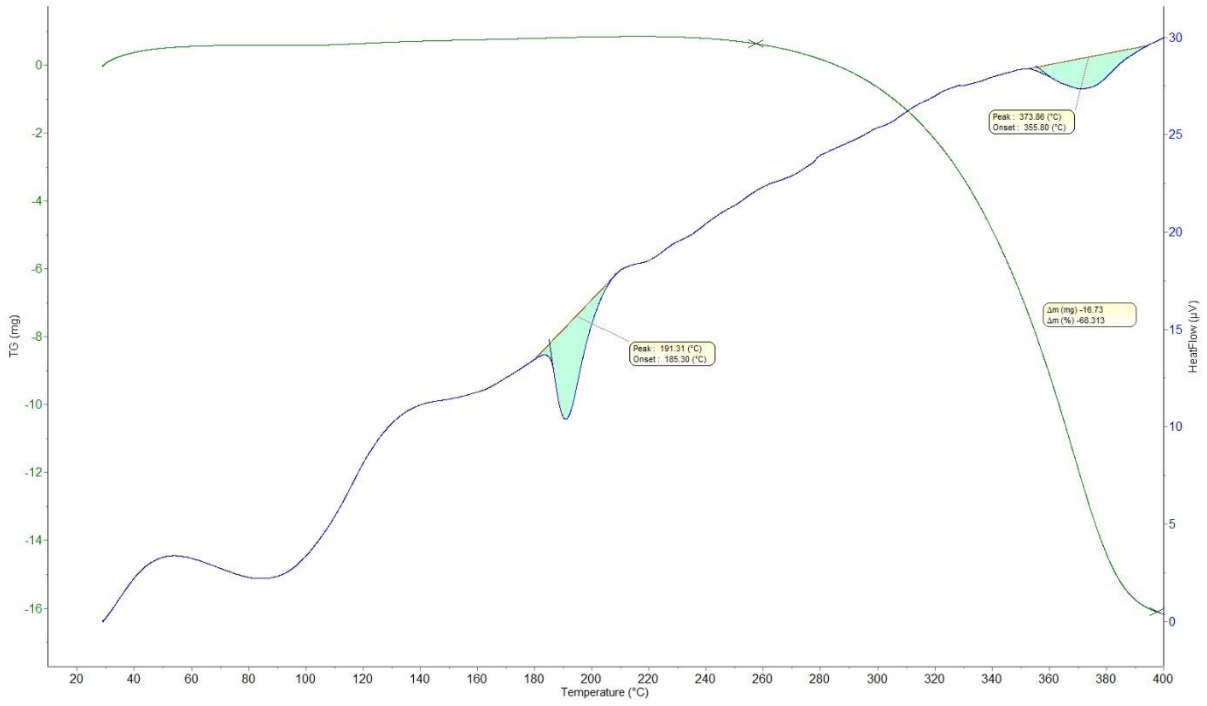

Figure S33: DTA/TG curve of **4**; the endothermic event between 60 and 120 °C is a known artifact of the apparatus used for the measurement and the endothermic event between 355 and 390 °C is caused by decomposition products. Decomposition of **4** starts at 260 °C with an overall mass loss of 68%.

5. Temperature dependent X-ray powder diffraction (XRPD) of 2 and 4

XRD data were collected in Debye-Scherrer geometry on a STOE STADI-P transmission diffractometer equipped with a curved Ge(111) monochromator and a linear position-sensitive detector (lin. PSD, Kr/CH_4). Cu-$K\alpha_1$ radiation (λ = 1.5406 Å) was used. About 10 mg of the samples were placed in glass capillaries, Ø = 0.7 mm (**2**)/0.5 mm (**4**), and sealed under Ar. The capillaries were mounted on the diffractometer and rotated during the measurements. The 2Θ range was 3 – 60 °, with a detector step width of 0.5 ° and a measurement time of 60 s/step, which corresponds in total to 720 s/step. The data were collected with the Stoe WinXPOW software.[S7] The temperature was controlled by an Oxford Cryosystem 600 device, using a steady flow of nitrogen, with a heating rate of 6 °C/ min.

Measurements of compound **2** were performed at 30 °C, in 20 °C steps from 60 °C up to 120 °C, and then in 10 °C steps starting at 120 °C up to 200 °C. Finally, the sample was cooled to 30 °C and measured again.

Measurements of compound **4** were performed at 30 °C, 80 °C, and 130 °C, then in 10 °C steps from 170 °C up to 220 °C. Finally, the sample was cooled to 30 °C and measured again.

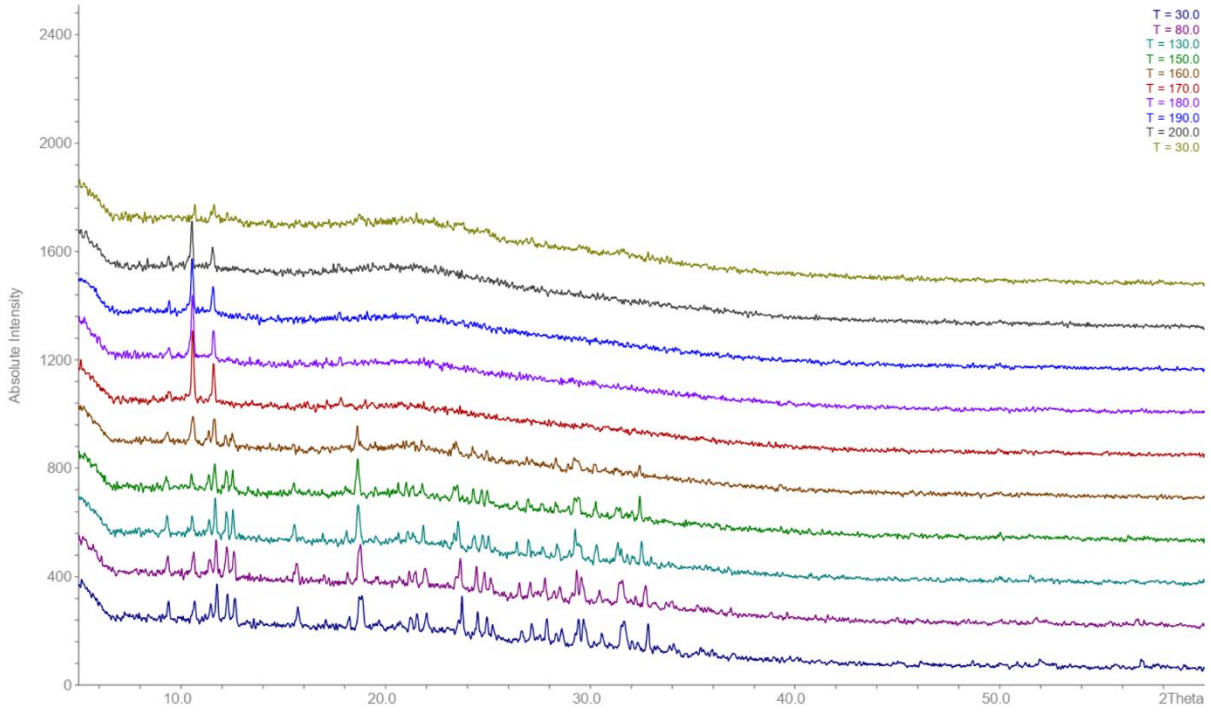

Figure S34: Temperature-dependent X-ray powder diffraction of **2** at room temperature (bottom) and selected elevated temperatures.

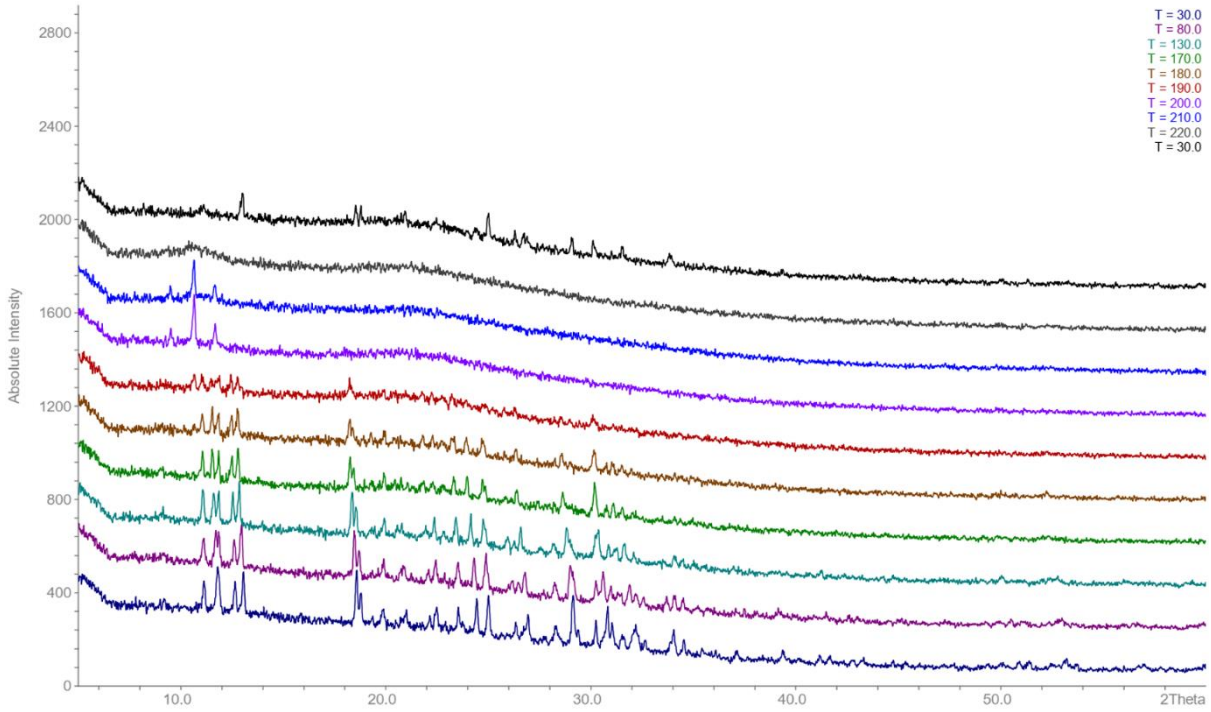

Figure S35: Temperature-dependent X-ray powder diffraction of **4** at room temperature (bottom) and selected elevated temperatures.

6. UV/vis absorption spectrum of [*n*Bu$_4$N]$_2$[1]

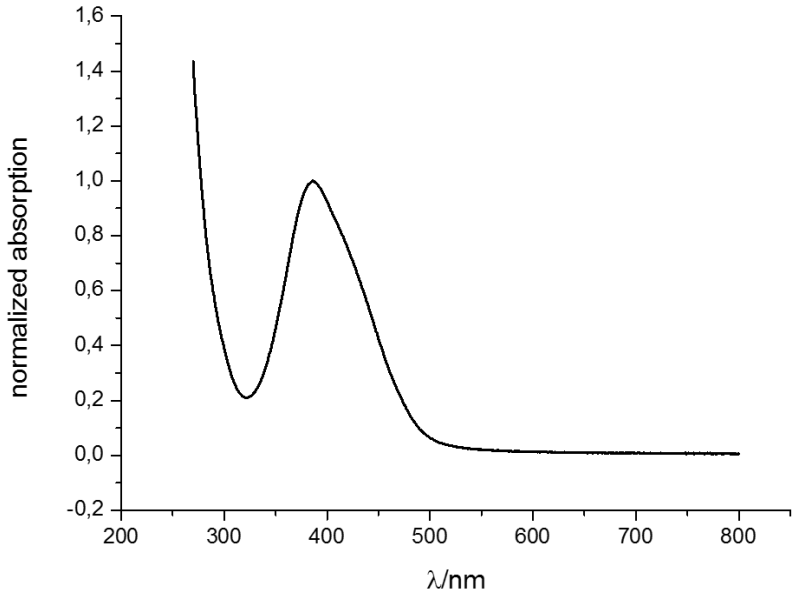

Figure S36: UV/vis absorption spectrum of [*n*Bu$_4$N]$_2$[**1**] in THF (c = 250 µM , λ_{max} = 386 nm).

7. Cyclic voltammogram of 4

The cyclic voltammogram of **4** in CH_2Cl_2 shows one reversible redox process at a potential value of $E_{1/2}$ = –1.78 V. *Note*: After about 8 sequential measurement cycles, **4** had decomposed to such an extent that the cyclic voltammogram no longer showed a reversible redox event.

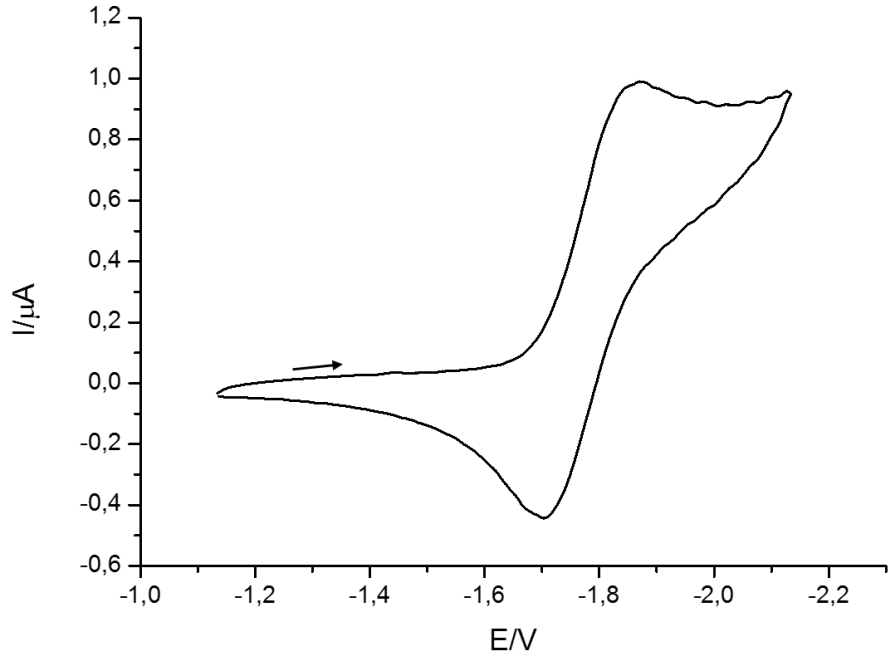

Figure S37: Cyclic voltammogram of **4** in CH_2Cl_2 at room temperature; vs. FcH/FcH+, supporting electrolyte: [nBu$_4$N][B(C$_6$F$_5$)] (0.05 M), scan rate: 200 mVs^{-1}.

8. Computational details

General remarks, geometry optimizations and single point energies

Structures were visualized with UCSF Chimera[S8] 1.10.2. Quantum-mechanical calculations were performed with the TURBOMOLE 7.3.1[S9,S10], ADF2019.303,[S11,S12] and xtb 6.2.3[S13] program packages. Geometries were pre-optimized with the GFN2-xTB[S14] extended tight binding method applying the generalized born solvation with solvent accessible surface (GBSA)[S15] model for CH_2Cl_2. Final geometries were optimized by applying the PBE0[S16] hybrid density functional in conjunction with the def2-TZVPD[S17] basis set including diffuse basis functions or the def2-TZVP[S18], the COSMO[S19] implicit continuum solvation model for CH_2Cl_2 (ε = 8.93), and the D4[S20,S21] London dispersion correction. The numerical quadrature grid m4[S22] was employed for the integration of the exchange-correlation contributions and default convergence criteria for energies and gradients were applied as implemented in TURBOMOLE. Minimum structures were verified as minima on the potential energy hyper surface by the absence of imaginary frequencies ($i\omega > 35$ cm^{-1}) in the harmonic vibrational frequency calculation. Imaginary frequencies below this threshold were inverted and included in the thermostatistical correction.

All geometry optimizations and single-point energy calculations were performed by applying the resolution-of-identity (RI) approximation for Coulomb integrals[S23] with matching default auxiliary basis sets.[S24]

Ro-vibrational corrections to obtain free energies were obtained from a modified rigid rotor harmonic oscillator statistical treatment[S25] (T = 25.0 °C, 1 atm pressure) based on harmonic frequencies calculated at the geometry optimization level. To avoid errors in the harmonic approximation, frequencies with wave numbers below 100 cm^{-1} were treated partially as rigid rotors.[S26]

Gas-phase single-point energies were calculated at the PBE0-D4/def2-QZVPPD[S17] or PBE0-D4/def2-QZVPP level by applying the m5 numerical quadrature grid.

Solvation corrections and Gibbs free energies

Solvation effects were further considered by the COSMO-RS[S26,S27] model, used as implemented in COSMOtherm (Version C3.0, release 16.01)[S28] with the 2016 parameterization for CH_2Cl_2 (parameter file: BP_TZVP_C30_1601.ctd; default G_{solv} option). Calculated solvation corrections were further corrected for the volume work of 1 bar to 1 M ideal gas. The default BP86[S29,S30]/def-TZVP[S31] level of theory was used for single-point calculations on the optimized geometries.

Final Gibbs free energies were obtained by summing the gas phase single-point energy E, the dispersion correction $E_{Disp.}$, the ro-vibrational correction G_{RRHO}, and the solvation correction $\delta G_{solv., corr.}$ (eq. S1).

$$G_{tot.} = E + E_{Disp., D4} + G_{RRHO} + \delta G_{solv., corr.} \quad \text{(equation S1)}$$

Tabulated energy contributions

Table S6. Tabulated energy contributions.

#	E(PBE0-D4 (COSMO(CH_2Cl_2)) /def2-TZVPD) / a.u.	E(PBE0/def2-QZVPPD) / a.u.	E(PBE0/def2-QZVPPD) / kcal·mol^{-1}	E_{Disp}(D4) / kcal·mol^{-1}	G_{RRHO} (25 °C) / kcal·mol^{-1}	$\delta G_{solv., corr.}$ (25 °C) / kcal·mol^{-1}	G_{tot} / kcal·mol^{-1}
[H**1**]^-_c	-10171.594960	-10171.738786	-6382862.458	-73.916	-0.300	-39.075	-6382975.749
[H**1**]^-_i	-10171.543621	-10171.688727	-6382831.046	-73.748	-0.682	-37.926	-6382943.402
[H**1**]^-_t	-10171.590327	-10171.736127	-6382860.790	-73.602	-0.832	-37.872	-6382973.096
TMS	-448.946631						

Table S7. Tabulated energy contributions for hypohomodesmotic reactions, **4** and TMS.

#	E(PBE0-D4 (COSMO(CH_2Cl_2)) /def2-TZVP) / a.u.	E(PBE0/def2-QZVPP) / a.u.	E(PBE0/def2-QZVPP) / kcal·mol^{-1}	E_{Disp}(D4) / kcal·mol^{-1}	H (25 °C) / kcal·mol^{-1}	G_{RRHO} (25 °C) / kcal·mol^{-1}	H_{tot} / kcal·mol^{-1}
$I_{C, open}$	-392.773908	-392.774974	-246470.017	-15.408	175.277	142.720	-246310.148
$I_{C, closed}$	-233.124873	-233.129376	-146290.892	-5.465	75.943	54.373	-146220.414
$I_{Si, open}$	-895.401146	-895.411882	-561879.439	-18.234	125.389	161.738	-561735.935
$I_{Si, closed}$	-735.805436	-735.821683	-461735.077	-7.442	64.312	39.979	-461678.207
Ethane	-79.753475	-79.757095	-50048.333	-1.376	47.134	30.841	-50002.574
4	-9250.589299	-9250.775307	-5804949.150	-62.233	58.802	-6.954	-5804952.580
TMS	-448.945979						

NMR chemical shift calculations

NMR chemical shifts δ for ^{1}H, ^{13}C, and ^{29}Si nuclei were calculated relative to tetramethylsilane (TMS) following equation S2:

$$\delta(^{X}) = \sigma(X_{TMS}) - \sigma(X) \text{ (equation S2)}$$

Isotropic chemical shielding constants σ were calculated by applying the ADF2019.303[S12,S32,S33] program package. The PBE0 functional was applied with the all-electron ZORA/QZ4P[S34] basis set and the zero-order regular approximation (ZORA)[S35,S36] including spin-orbit corrections (SO-ZORA)[S37]. The COSMO[S38] implicit solvation model was applied for CH_2Cl_2 (*surf Esurf, solv Eps=8.93 Rad=1.3*; *div ndiv=5* settings). Otherwise, default settings including gauge-including atomic orbital (GIAO) were applied as implemented in ADF2019.303.

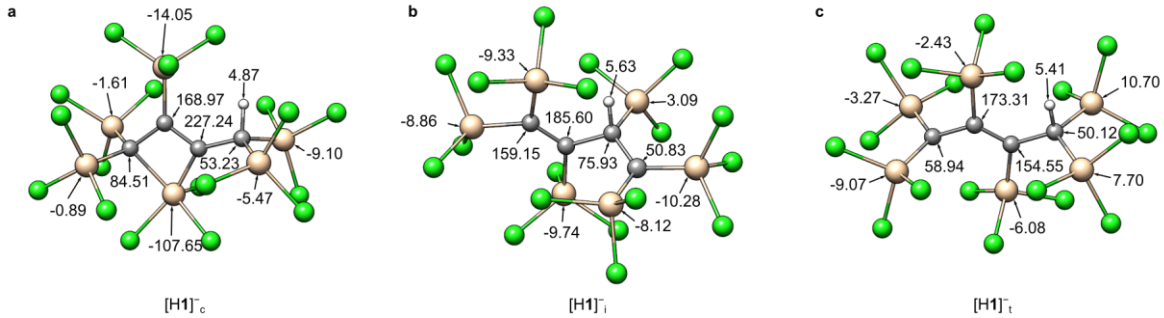

Figure S38. Calculated chemical shifts of $[H\mathbf{1}]^-_c$, $[H\mathbf{1}]^-_t$, and $[H\mathbf{1}]^-_i$ in ppm with TMS as reference at the SO-ZORA-PBE0(COSMO(CH_2Cl_2))/ZORA/QZ4P//PBE0-D4(COSMO(CH_2Cl_2))/def2-TZVPD level of theory. *Note:* For comparison with the NMR data provided in Figure S1, the chemical shift values of symmetry-related atoms (assuming a freely rotating molecule in solution) should be averaged.

Table S8. Calculated NMR parameters for TMS at the SO-ZORA-PBE0(COSMO(CH_2Cl_2))/ZORA/QZ4P level (X) of theory on PBE0-D4(COSMO(CH_2Cl_2))/def2-TZVPD and def2-TZVP geometries.

	TMS		
		σ / ppm	
Element	**Atom No.**	def2-TZVPD	def2-TZVP
H	3	31.29	31.30
H	4	31.29	31.30
H	5	31.29	31.30
H	7	31.29	31.29
H	8	31.30	31.30
H	9	31.30	31.30
H	11	31.29	31.29
H	12	31.30	31.30
H	13	31.30	31.30
H	15	31.29	31.30
H	16	31.29	31.30
H	17	31.30	31.30
C	2	187.22	187.21
C	6	187.23	187.22
C	10	187.23	187.22
C	14	187.22	187.21
Si	1	349.96	349.84

Table S9. Calculated ^{29}Si NMR parameters for $[H\mathbf{1}]^-_c$, $[H\mathbf{1}]^-_i$, and $[H\mathbf{1}]^-_t$ at the SO-ZORA-PBE0(COSMO(CH_2Cl_2))/ZORA/QZ4P//PBE0-D4(COSMO(CH_2Cl_2))/def2-TZVPD level of theory.

	$[H\mathbf{1}]^-_c$			$[H\mathbf{1}]^-_i$			$[H\mathbf{1}]^-_t$		
Element	**Atom No.**	**σ / ppm**	**δ / ppm**	**Atom No.**	**σ / ppm**	**δ / ppm**	**Atom No.**	**σ / ppm**	**δ / ppm**
H	23	26.42	4.87	17	25.66	5.63	18	25.88	5.41
C	1	102.72	84.51	1	28.08	159.15	1	128.29	58.94
C	2	18.26	168.97	2	1.63	185.60	2	13.92	173.31
C	3	-40.01	227.24	3	111.30	75.93	3	32.68	154.55
C	17	134.00	53.23	4	136.40	50.83	4	137.11	50.12
Si	4	457.61	-107.65	5	358.82	-8.86	5	352.39	-2.43
Si	5	350.85	-0.89	9	359.29	-9.33	9	356.04	-6.08
Si	9	351.57	-1.61	13	359.70	-9.74	13	342.26	7.70
Si	13	364.01	-14.05	18	346.87	3.09	17	339.26	10.70
Si	18	355.43	-5.47	22	360.24	-10.28	22	359.03	-9.07
Si	22	359.06	-9.10	26	358.08	-8.12	26	353.23	-3.27

Table S10. Calculated NMR parameters for **4** at the SO-ZORA-PBE0(COSMO(CH_2Cl_2))/ZORA/QZ4P//PBE0-D4(COSMO(CH_2Cl_2))/def2-TZVP level of theory.

	4		
Element	**Atom No.**	**σ / ppm**	**δ / ppm**
C	1	127.37	59.85
C	2	1.54	185.68
C	14	127.61	59.61
C	15	1.51	185.71
Si	3	347.93	1.91
Si	4	350.70	-0.86
Si	5	361.66	-11.82
Si	16	347.86	1.98
Si	17	350.70	-0.86
Si	18	361.76	-11.92

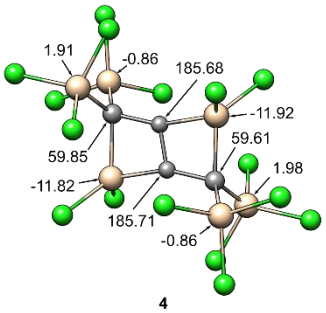

Figure S39. Calculated chemical shifts for **4** in ppm with TMS as reference at the SO-ZORA-PBE0(COSMO(CH_2Cl_2))/ZORA/QZ4P//PBE0-D4(COSMO(CH_2Cl_2))/def2-TZVP level of theory.

[H**1**]$^{-}_{t}$

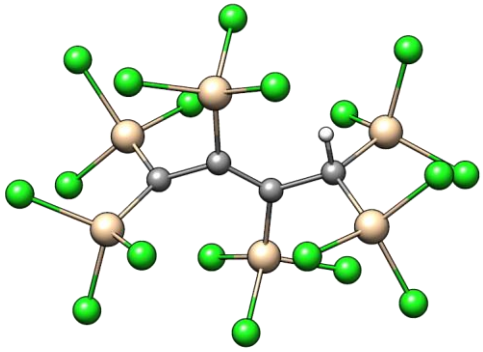

C	–1.8436384	–0.5898452	–0.4191433
C	–0.5994697	0.2095808	–0.3686584
C	0.4938286	–0.1850772	0.323085
C	1.7758849	0.6207837	0.3602551
Si	–0.6487319	1.7318405	–1.4929667
Cl	–2.547305	2.3714212	–1.8287813
Cl	0.1727871	1.1700505	–3.2810758
Cl	0.3507982	3.4419265	–0.9145178
Si	0.3277935	–1.7230649	1.3856699
Cl	–0.5506194	–3.4517385	0.7745791
Cl	–0.5067855	–1.1627245	3.1633902
Cl	2.239362	–2.3469444	1.8408561
Si	2.1659057	1.5689366	1.9393579
Cl	3.5240681	3.0032765	1.4208117
Cl	2.9376194	0.5465607	3.5126526
Cl	0.4758856	2.4825083	2.5928404
Si	3.2649996	–0.0751741	–0.5641457
H	1.6089707	1.5116153	–0.2645611
Cl	4.9069539	–0.4384078	0.5844592
Cl	3.8285318	1.3355711	–1.9334092
Cl	2.7822343	–1.750918	–1.5985766
Si	–3.2318476	–0.1888314	0.6254015
Cl	–2.8427551	1.4885353	1.7546049
Cl	–3.8136451	–1.6353843	1.9869444
Cl	–5.0182661	0.1820366	–0.3591677
Si	–2.1835628	–1.6477382	–1.8146125
Cl	–3.0831638	–0.7957337	–3.4840773
Cl	–3.4905638	–3.1640101	–1.3275252
Cl	–0.4952693	–2.5090512	–2.6136894

[H**1**]$^{-}{}_{c}$

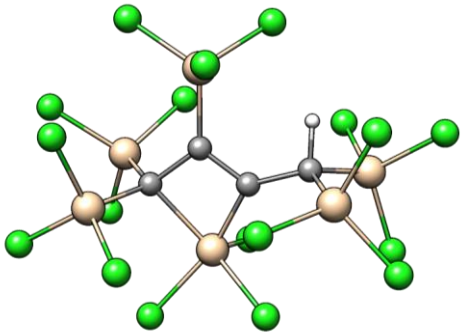

C	–1.8099994	–0.1588753	0.1713345
C	–0.5390371	0.3512981	–0.5108677
C	0.5095506	–0.1452579	0.1841155
Si	–0.5202267	–1.1801664	1.4246132
Si	–2.7386161	1.1322385	1.1230363
Cl	–1.6773712	1.7952254	2.7369341
Cl	–4.5628204	0.4950597	1.7808702
Cl	–3.0884704	2.8247433	0.0201506
Si	–2.8975967	–1.2260673	–0.8972903
Cl	–1.7870898	–1.9245972	–2.4678778
Cl	–4.5038276	–0.2458926	–1.7263152
Cl	–3.7357408	–2.8260112	0.0450852
Si	–0.3522326	1.4505453	–2.0069867
Cl	–2.0400075	1.7611452	–3.0921187
Cl	1.0079688	0.7014109	–3.3455096
Cl	0.3798722	3.2635472	–1.410918
C	1.9651509	0.0654853	–0.0873384
Si	2.8763833	1.258121	1.0567458
Cl	1.6124866	2.4622576	2.0834918
Cl	3.992649	2.487065	–0.1458416
Cl	4.183708	0.4009792	2.3592149
Si	2.9384222	–1.4852088	–0.5186502
H	2.0842865	0.608741	–1.0385077
Cl	2.0171248	–2.4765309	–2.0342828
Cl	3.2909335	–2.7924247	0.9880739
Cl	4.7561978	–0.8664652	–1.2230857
Cl	0.9252524	–0.9604903	3.0059995
Cl	–0.2457102	–3.0955126	0.6473053
Cl	–2.0412401	–1.6743622	2.8786197

[H**1**]$^{-}{}_{i}$

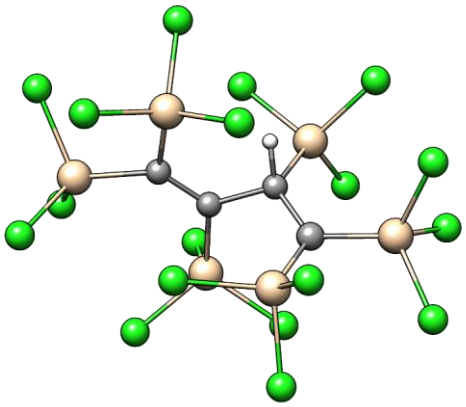

C	–1.6291841	–0.7718029	–0.1812906
C	–0.8224977	0.3013802	0.0384492
C	0.5413405	0.1013876	0.6598627
C	1.7201198	0.4344159	–0.2324782
Si	–3.430266	–0.7769094	–0.7159569
Cl	–4.5673737	0.8344997	–0.2211485
Cl	–4.3745101	–2.3018758	0.2696232
Cl	–3.6402228	–1.0494607	–2.7228538
Si	–0.9653644	–2.5470606	0.0002195
Cl	1.0215944	–2.9177005	–0.3111202
Cl	–1.8503202	–3.7325215	–1.4143874
Cl	–1.3742015	–3.3286578	1.8414961
Si	–1.241132	2.1175031	–0.3770157
Cl	–2.1282703	2.2263784	–2.2041206
Cl	0.3542025	3.3682203	–0.4338141
Cl	–2.4447311	2.9330841	1.0551293
H	0.5794387	–0.9653661	0.9676705
Si	0.3868315	0.6280966	2.4992158
Cl	0.4656074	2.5839099	3.0543306
Cl	1.767239	–0.4330516	3.560871
Cl	–1.4328035	–0.0295222	3.1680628
Si	3.3696411	0.7151797	0.3922878
Cl	4.6765835	1.4720508	–1.0117597
Cl	4.3475987	–0.9737578	1.1100841
Cl	3.556689	2.070726	1.9374591
Si	1.7528647	0.1219089	–1.9999403
Cl	0.0692621	–0.6896807	–2.8881261
Cl	3.2437305	–1.1832311	–2.638588
Cl	2.048134	1.7918576	–3.2021615

Tetramethylsilane (def2-TZVPD)

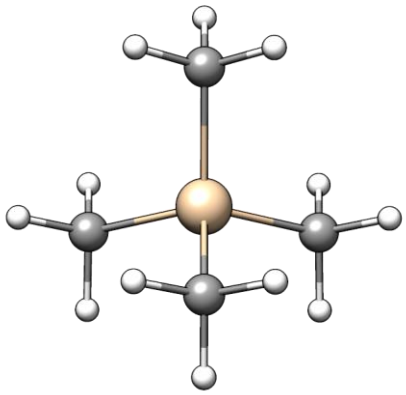

Si	0	0	0
C	–1.0826712	–1.0826712	–1.0826712
H	–1.7258739	–1.7258739	–0.4750621
H	–0.4750621	–1.7258739	–1.7258739
H	–1.7258739	–0.4750621	–1.7258739
C	1.0826712	1.0826712	–1.0826712
H	1.7258739	1.7258739	–0.4750621
H	0.4750621	1.7258739	–1.7258739
H	1.7258739	0.4750621	–1.7258739
C	–1.0826712	1.0826712	1.0826712
H	–0.4750621	1.7258739	1.7258739
H	–1.7258739	0.4750621	1.7258739
H	–1.7258739	1.7258739	0.4750621
C	1.0826712	–1.0826712	1.0826712
H	1.7258739	–0.4750621	1.7258739
H	1.7258739	–1.7258739	0.4750621
H	0.4750621	–1.7258739	1.7258739

Tetramethylsilane (def2-TZVP)

Si	0.0000058	–0.0000035	0.0000016
C	–1.0830542	–1.0830486	–1.0830511
H	–1.7259971	–1.7259327	–0.4750185
H	–0.4750543	–1.7260043	–1.7259474
H	–1.7259345	–0.4750109	–1.7259847
C	1.0830518	1.0830524	–1.0830498
H	1.7259954	1.7259318	–0.4750097
H	0.4750487	1.7260057	–1.7259411
H	1.7259248	0.475026	–1.7259965
C	–1.0830517	1.0830444	1.0830465
H	–0.4750255	1.7260038	1.7259182
H	–1.7259336	0.4750333	1.7260042
H	–1.7260073	1.7259037	0.4750191
C	1.0830565	–1.0830497	1.0830494
H	1.7259331	–0.4750218	1.7259975
H	1.7260169	–1.7259316	0.4750471
H	0.475025	–1.7259983	1.7259152

3,4-Diethylhex-3-en ($I_{C,\ open}$)

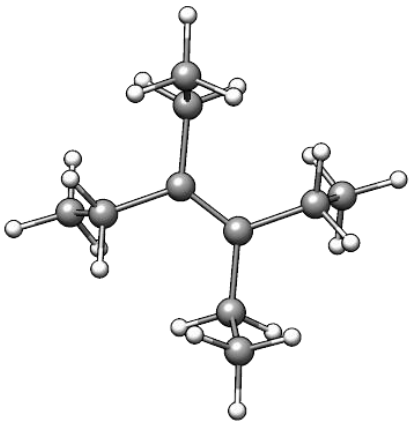

C	–0.6692844	–0.0001802	–0.0000487
C	0.6693876	–0.0000198	0.0000621
C	1.4868273	–1.2643419	0.005234
C	1.912901	–1.676493	1.4117049
H	2.5572283	–2.5593296	1.3889225
H	1.0394925	–1.9067941	2.0270433
H	2.4638158	–0.8731694	1.9079191
H	0.9447421	–2.0864602	–0.4663717
H	2.3838113	–1.1050895	–0.6040946
C	1.4865059	1.2645153	–0.0049607
C	1.9122367	1.6770935	–1.411409
H	2.5563642	2.560074	–1.3885339
H	1.0386677	1.9073366	–2.0265402
H	2.463247	0.8740101	–1.9079064
H	0.9442874	2.086388	0.4669252
H	2.3836315	1.1053621	0.6041801
C	–1.4864414	–1.2646874	–0.0049774
C	–1.912402	–1.6771914	–1.4113778
H	–2.4633093	–0.8739973	–1.9078109
H	–1.0389508	–1.9075837	–2.0266199
H	–2.5566949	–2.5600553	–1.3884264
H	–2.3834859	–1.1054861	0.6042688
H	–0.9442157	–2.0865851	0.4668589
C	–1.4867116	1.2641502	0.0046834
C	–1.9127398	1.6768546	1.4110044
H	–1.0393172	1.9073677	2.0262357
H	–2.46367	0.8737494	1.9075588
H	–2.5570265	2.5597137	1.3878875
H	–0.9446575	2.0860663	–0.4673114
H	–2.3837323	1.1046558	–0.6045308

$\Delta^{1,4}$-Bicyclo[2.2.0]hexene ($I_{C,\ closed}$)

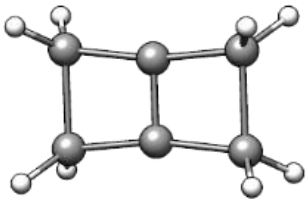

C	0.3554604	–0.4511141	–1.6129028
C	–0.2267011	–0.5792228	–0.212131
C	0.8972054	0.9550958	–1.1018587
H	1.9873843	1.0372983	–1.0834054
H	0.4883952	1.8170689	–1.6361707
C	–0.3561778	0.4514888	1.6126245
C	0.2204951	0.5824253	0.2098508
C	–0.8976105	–0.9548852	1.1017148
H	–1.9876062	–1.0402958	1.0879088
H	–0.4839836	–1.8162658	1.6332817
H	–0.3606683	–0.386052	–2.4366146
H	0.3637815	0.3852292	2.4329031
H	1.1392865	–1.1637571	–1.8837911
H	–1.139261	1.1629863	1.8885904

Ethane

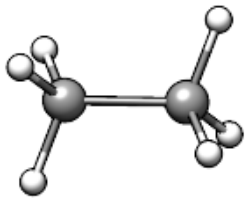

C	–0.2569652	0.714941	0.0000046
H	0.0874833	1.2613147	–0.8816954
C	0.2569754	–0.7149379	0.0000046
H	0.0875894	1.2613796	0.8816223
H	–0.0874921	–1.261299	–0.8816965
H	–0.0875982	–1.261364	0.8816234
H	1.3495148	–0.7448014	0.0000685
H	–1.3495071	0.7447671	0.0000685

3,4-Di(methylsily)hex-3-en ($I_{Si,\ open}$)

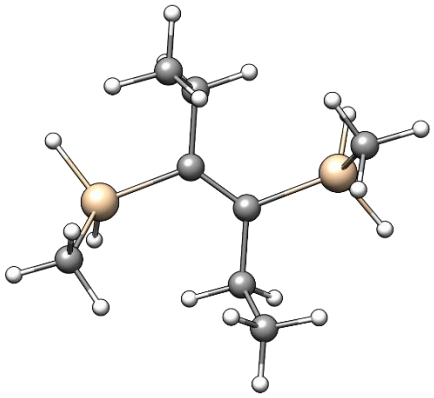

C	0.4702122	0.4805846	0.5110253
Si	2.3138067	0.0837798	0.5137617
H	3.0297284	1.3654776	0.7821163
H	2.6545594	–0.8371347	1.6370464
C	2.9351354	–0.6388753	–1.0968532
H	4.0190097	–0.7742219	–1.0591581
H	2.6988064	0.0275497	–1.9297867
H	2.4748605	–1.6087603	–1.2964702
C	–0.4703082	–0.4806303	0.5111283
Si	–2.3138977	–0.083809	0.5140535
H	–3.0298316	–1.3655035	0.7823917
H	–2.6545605	0.837066	1.637395
C	–2.9352898	0.638923	–1.0965035
H	–2.6997058	–0.0278661	–1.9293567
H	–2.4743925	1.6084262	–1.2965246
H	–4.0190571	0.7750389	–1.0585018
C	–0.1305238	–1.9475351	0.4705036
C	–0.4901114	–2.5848313	–0.8679341
H	–0.2381589	–3.6477632	–0.8752118
H	0.0454623	–2.0973992	–1.6860828
H	–1.5605564	–2.4966904	–1.0745674
H	0.9338895	–2.1061544	0.6749775
H	–0.6722225	–2.4712771	1.2667426
C	0.1304367	1.9474955	0.4704623
C	0.4904247	2.5849765	–0.8677776
H	0.2384732	3.6479093	–0.8749731
H	–0.0448983	2.0976641	–1.6861623
H	1.5609333	2.4968674	–1.0740977
H	–0.9340368	2.1060893	0.6746414
H	0.6718969	2.4711309	1.2669359

2,5-Disilabicyclo[2.2.0]hex-1(4)-ene ($I_{Si,\ closed}$)

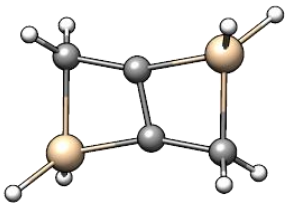

C	0.220894	1.7181954	7.7286511
C	–0.3118593	1.6923308	9.1435252
Si	0.9114138	3.420003	8.247353
H	2.3948877	3.5669539	8.2908545
H	0.365044	4.6172179	7.5458704
C	–0.4904036	2.8097937	11.2059416
C	0.0424459	2.8356075	9.7911034
Si	–1.1829516	1.109031	10.6864649
H	–2.6666113	0.9658212	10.6410031
H	–0.6404535	–0.0897755	11.3884496
H	–0.5509678	1.7092666	6.956161
H	0.2813677	2.8180893	11.9785133
H	0.9466354	0.9332569	7.5054792
H	–1.2155316	3.5952683	11.4292899

4

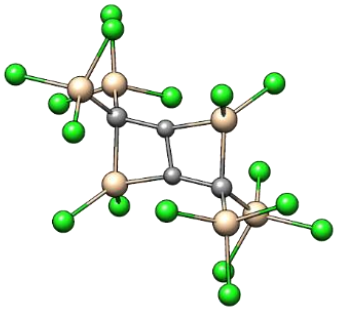

C	0.3235828	–0.6236956	–1.7392084
C	–0.1269077	–0.6011373	–0.292697
Si	1.6507377	–1.8865451	–2.1729158
Si	–1.1615967	–0.7153452	-2.8839647
Si	0.9974734	1.1274683	–1.243314
Cl	0.9020556	–3.6540289	–2.8386777
Cl	2.8491792	–1.1470234	–3.6354279
Cl	2.7499254	–2.3073446	–0.5212129
Cl	–0.5564143	–0.7401301	–4.8184577
Cl	–2.2501376	–2.3805933	–2.4674893
Cl	–2.4276038	0.8459567	–2.6165828
Cl	3.0117576	1.2451113	–1.0283918
Cl	0.4125753	2.7513476	–2.2967929
C	–0.323567	0.6237706	1.7394588
C	0.1271225	0.6010625	0.2930276
Si	–1.6494826	1.8881443	2.1723741
Si	1.16133	0.7132121	2.8847083
Si	–0.9983805	–1.1269237	1.2432559
Cl	–0.898615	3.6546533	2.8382319
Cl	–2.8501357	1.1508389	3.634114
Cl	–2.7467894	2.3100402	0.5196614
Cl	0.5549257	0.7371738	4.8188841
Cl	2.2524851	2.3772033	2.4703557
Cl	2.4254825	–0.8494783	2.6165273
Cl	–3.0127818	–1.2419718	1.0277125
Cl	–0.4162205	–2.7517655	2.2968212

9. References

[S1] G. R. Fulmer, A. J. M. Miller, N. H. Sherden, H. E. Gottlieb, A. Nudelman, B. M. Stoltz, J. E. Bercaw, K. I. Goldberg, *Organometallics* **2010**, *29*, 2176–2179.

[S2] J. Tillmann, L. Meyer, J. I. Schweizer, M. Bolte, H.-W. Lerner, M. Wagner, M. C. Holthausen, *Chem. Eur. J.* **2014**, *20*, 9234–9239.

[S3] I. Georg, J. Teichmann, M. Bursch, J. Tillmann, B. Endeward, M. Bolte, H.-W. Lerner, S. Grimme, M. Wagner, *J. Am. Chem. Soc.* **2018**, *140*, 9696–9708.

[S4] R. R. Gupta, M. D. Lechner, Eds., *Chemical Shifts and Coupling Constants for Silicon-29*, Springer, Berlin, Heidelberg, **2008**.

[S5] Stoe & Cie., *X-AREA. Diffractometer Control Program System*, Stoe & Cie, Darmstadt, Germany, **2002**.

[S6] G. M. Sheldrick, *Acta Crystallogr. Sect. A: Found. Crystallogr.* **2008**, *64*, 112–122.

[S7] *STOE WinXPOW 310*, Stoe & Cie GmbH, Darmstadt, Germany, **2016**.

[S8] E. F. Pettersen, T. D. Goddard, C. C. Huang, G. S. Couch, D. M. Greenblatt, E. C. Meng, T. E. Ferrin, *J. Comput. Chem.* **2004**, *25*, 1605–1612.

[S9] F. Furche, R. Ahlrichs, C. Hättig, W. Klopper, M. Sierka, F. Weigend, *Wiley Interdiscip. Rev. Comput. Mol. Sci.* **2014**, *4*, 91–100.

[S10] *TURBOMOLE V7.3.1 2018*, a Development of the University of Karlsruhe and Forschungszentrum Karlsruhe GmbH, 1989-2007, TURBOMOLE GmbH, since **2007**, available from http://www.turbomole.com.

[S11] G. te Velde, F. M. Bickelhaupt, E. J. Baerends, C. Fonseca Guerra, S. J. A. van Gisbergen, J. G. Snijders, T. Ziegler, *J. Comput. Chem.* **2001**, *22*, 931–967.

[S12] ADF 2019.3, SCM, Theoretical Chemistry, Vrije Universiteit, Amsterdam, The Netherlands, http://www.scm.com.

[S13] Semiempirical Extended Tight-Binding Program Package Xtb, Version 6.2, https://github.com/Grimme-Lab/Xtb. Accessed: 2020-05-03.

[S14] C. Bannwarth, S. Ehlert, S. Grimme, *J. Chem. Theory Comput.* **2019**, *15*, 1652–1671.

[S15] W. Clark Still, A. Tempczyk, R. C. Hawley, T. Hendrickson, *J. Am. Chem. Soc.* **1990**, *112*, 6127–6129.

[S16] C. Adamo, V. Barone, *J. Chem. Phys.* **1999**, *110*, 6158–6170.

[S17] D. Rappoport, F. Furche, *J. Chem. Phys.* **2010**, *133*, 134105–11.

[S18] F. Weigend, R. Ahlrichs, *Phys. Chem. Chem. Phys.* **2005**, *7*, 3297–3305.

[S19] A. Klamt, G. Schüürmann, *J. Chem. Soc. Perkin Trans. 2* **1993**, 799–805.

[S20] E. Caldeweyher, C. Bannwarth, S. Grimme, *J. Chem. Phys.* **2017**, *147*, 034112–7.

[S21] E. Caldeweyher, S. Ehlert, A. Hansen, H. Neugebauer, S. Spicher, C. Bannwarth, S. Grimme, *J. Chem. Phys.* **2019**, *150*, 154122.

[S22] K. Eichkorn, F. Weigend, O. Treutler, R. Ahlrichs, *Theor. Chem. Acc.* **1997**, *97*, 119–124.

[S23] K. Eichkorn, O. Treutler, H. Öhm, M. Häser, R. Ahlrichs, *Chem. Phys. Lett.* **1995**, *240*, 283–290.

[S24] F. Weigend, *Phys. Chem. Chem. Phys.* **2006**, *8*, 1057–1065.

[S25] S. Grimme, *Chem. Eur. J.* **2012**, *18*, 9955–9964.

[S26] A. Klamt, *J. Phys. Chem.* **1995**, *99*, 2224–2235.

[S27] F. Eckert, A. Klamt, *AIChE J.* **2002**, *48*, 369–385.

[S28] A. Klamt, F. Eckert, L. Pohler, *COSMOtherm*. COSMOlogic GmbH & Co. KG: Leverkusen, Germany **2013**.

[S29] A. D. Becke, *Phys. Rev. A* **1988**, *38*, 3098–3100.

[S30] J. P. Perdew, *Phys. Rev. B* **1986**, *33*, 8822–8824.

[S31] A. Schäfer, C. Huber, R. Ahlrichs, *J. Chem. Phys.* **1994**, *100*, 5829–5835.

[S32] G. Schreckenbach, T. Ziegler, *J. Phys. Chem.* **1995**, *99*, 606–611.

[S33] M. Krykunov, T. Ziegler, E. van Lenthe, *Int. J. Quantum Chem.* **2009**, *109*, 1676–1683.

[S34] E. van Lenthe, E. J. Baerends, *J. Comput. Chem.* **2003**, *24*, 1142–1156.

[S35] E. van Lenthe, E. J. Baerends, J. G. Snijders, *J. Chem. Phys.* **1993**, *99*, 4597–4610.

[S36] E. van Lenthe, E. J. Baerends, J. G. Snijders, *J. Chem. Phys.* **1994**, *101*, 9783–9792.

[S37] E. van Lenthe, J. G. Snijders, E. J. Baerends, *J. Chem. Phys.* **1996**, *105*, 6505–6516.

[S38] C. C. Pye, T. Ziegler, *Theor. Chem. Acc.* **1999**, *101*, 396–408.